PHOTOSYNTHETICALLY AVAILABLE RADIATION (PAR)

IN THE COLORADO RIVER: GLEN AND GRAND CANYON

DRAFT REPORT

ORIGINAL

January 11, 1993

GCES OFFICE COPY
DO NOT REMOVE!

Michael D. Yard
George A. Haden
William S. Vernieu

Glen Canyon Environmental Studies
P.O. Box 22459
Flagstaff, Arizona 86002-2459
(602) 556-7363

DRAFT

TABLE OF CONTENTS

LIST OF TABLES

LIST OF FIGURES

Photosynthetically Available Radiation (PAR)

in the Colorado River: Glen and Grand Canyon

ABSTRACT

Photosynthetically available radiation (PAR) is a limiting factor on primary productivity and growth of aquatic algae in the Colorado River of Glen and Grand Canyons. The primary component contributing to light attenuation is suspended sediment which reduces the spatial extent of PAR in depth and distance downstream under varying discharges at Glen Canyon Dam. A longitudinally stratified sampling approach was used to characterize the optical properties influencing light attenuation. Our analysis indicates light attenuation increases from Glen Canyon to Diamond Creek and is significantly related to increasing sediment concentrations that occur with increasing distance downstream and discharges measured at 142 and 425 m^3/s. At these constant discharges sediment amplification results from increasing downstream distances, fluvial hydrology and local geomorphology. Under high water clarity conditions with no sediment contribution from tributaries the compensation point for Cladophora glomerata ranges in depth from 19.4 to 3.6 m.

Acronyms and Symbols

a	= Absorptance coefficient	I	= Incidental light intensity (m^2/s)
b	= Total scattering coefficient	I_{ss}	= Sub-surface intensity (m^2/s)
b_b	= Normal backscattering coefficient	T_n	= Nephelometric turbidity unit (NTU)
b'_b	= Asymptotic backscattering coefficient	PAR	= Photosynthetically available radiation
E	= Net downward irradiance ($E_d - E_u$)	R_∞	= Asymptotic reflectance
E_d	= Downward irradiance	Q_s	= Suspended sediment concentration (g/L)
E_u	= Upward reflectance	Z_{cp}	= Compensation point depth
E_o	= Scalar irradiance	Z_{eu}	= Euphotic zone depth (1% of PAR)
K	= Vertical attenuation coefficient	Z_m	= Euphotic zone depth (10% of PAR)
K_{avg}	= Average vertical attenuation coefficient	Z_{SD}	= Secchi disc depth
K_d	= Attenuation coefficient for cosine irradiance	μE	= Microeinsteins (m^2/s), ($6.02 \cdot 10^{17}$ quanta)
K_o	= Attenuation coefficient for scalar irradiance	K_E	= Attenuation coefficient for net irradiance

INTRODUCTION

Photosynthetically available radiation, *PAR* (400-700 nm wavelength), is critical to underwater photosynthesis and its subsequent productivity. Numerous factors which influence primary production and the proportional growth of algae in aquatic ecosystems include nutrient loads (Mantai 1978), temperature (Hodgson 1981), channel geomorphology (Tett *et al.* 1978), suspended sediment loads (Jewson and Taylor 1978), and seasonal light variation (Adams and Stone 1973; Graham *et al.* 1982). In this study we characterized spatially the light attenuation in the Colorado River, Glen and Grand Canyons, Arizona. The primary goal was to determine if under periods of minimal tributary discharge subsurface light availability was influenced by normal operations at Glen Canyon Dam.

Background Information

Prior to completion of Glen Canyon Dam in 1963, suspended sediment loads in the Colorado River in Glen and Grand canyons, exceeded 10,000 ppm (Dolan *et al.* 1974; Schmidt and Graf 1990). The operation of Glen Canyon Dam has since regulated flows and decreased sediment transport in the Colorado River (Pemberton 1976; Howard and Dolan 1981). The impoundment of Lake Powell and the resulting high clarity discharge abruptly shifted a previously allochthonous system of transported inorganic and organic material to an autotrophically based ecosystem. At present, tributary discharge of sediment into the Colorado River periodically shifts this relatively new riverine ecosystem into a quasi pre-dam environment.

Frequency, duration, and magnitude of tributary floods in the Grand Canyon are unpredictable, and their downstream extent and residency are quite variable (Webb 1987). These events can result in suspension of fine sands, colloidal silts, and clays which thereby partially or totally eliminate light penetration through the water surface. Suspended sediment loads are contributed to the river in three ways: 1) seasonal sediment input from perennial stream flow from the primary tributaries of

the Paria River, Little Colorado River, and Kanab Creek (Graf *et al.* 1990, Herford 1984); 2) infrequent flood and debris flow events from ephemeral drainage basins, (Webb 1987); and 3) degradation of alluvial deposits, (Schmidt and Graf 1990).

Problem Statement

Light availability becomes a critical aspect since the basal portion of the present aquatic productivity is derived primarily from photosynthesis (Usher *et al.* 1987; Hardwick *et al.* 1992). The degree of water clarity in the Colorado River and the resulting light penetration is inversely related to the presence of suspended sediment, and is functionally governed by sediment contribution from major tributaries, episodic events from ephemeral drainages and washes, and the degradation of alluvial deposits. The unpredictable and periodic nature of flood events is the primary factor limiting light availability in the Colorado River.

This research has primarily focused on secondary light attenuation, which results from degraded alluvium during periods of optimum water clarity conditions under normal operational discharges at Glen Canyon Dam. Irradiametric measurements were collected during periods of limited sediment contribution from tributaries, however, the proportion of light available for photosynthesis progressively decreased with increasing distances from Glen Canyon Dam. Scott (1978) conducted irradiametric studies in marine estuaries experiencing periodic sediment contribution and approached this problem by assuming that differences in measured attenuation coefficients, K , from the mean or optimum attenuation coefficient, K_{avg} , were proportionally related to increasing levels of suspended sediment. The observed changes from a base attenuation value K_{avg} was attributed to periodic input of sediment from adjacent river systems. Conceptually, the same assumption holds true for the Colorado River where increased light attenuation is the result of changes in sediment concentration. However, in our study changes in sediment concentration are related to the suspension and transport of degraded alluvium and not tributary flow.

Transmission of light and its vertical dispersal through water is directly influenced by the optical properties controlling light attenuation, absorptance and scattering (Di Toro 1978; Kirk 1980a; Kirk 1980b; and Kirk 1983). Concentration of suspended sediment, size distribution, shape, and refractive indices affect the orientation and distance that light travels through water, and ultimately its attenuation (Spinrad *et al.* 1978). This scattering aspect further intensifies the degree of light attenuation with depth (Kirk 1980b). Decreasing intensities with increasing depth are an outcome of both the absorptive (Kirk 1980b) and scattering characteristics of water (Kirk 1977; Kirk 1980a). Vertical attenuation coefficients increase in turbid waters as a result of the increased absorption and scattering properties of suspended sediment.

Information from this study will assist researchers investigating aquatic productivity in the Colorado River by bridging the span between light availability, assimilation and energy transformation through the series of trophic levels. In coordination with other research in progress this paper identifies additional factors related to primary production in the Colorado River.

Objectives

1. Determine if vertical light attenuation is significantly correlated to suspended sediment, discharge volume, and distance from Glen Canyon Dam.

2. Determine if photosynthetically available radiation, *PAR* , at variable discharges of 142 and 425 m^3/s varies spatially throughout the longitudinal extent of the Colorado River, Glen and Grand Canyons.

3. Determine the degree of scattering and absorptance to light attenuation for the Colorado River at variable discharges.

4. Determine the depth zonation of available light intensities (μE) for Cladophora glomerata at varying discharges in the Colorado River downstream from Glen Canyon Dam.

5. Determine if vertical attenuation coefficients, K , derived for downward and scalar irradiance are either equivalent or can be made equivalent.

6. Develop a method to correlate secchi depth measurements, Z_{SD} , to vertical light attenuation.

MATERIALS AND METHODS

Study Area

The study area is located on the Colorado Plateau of Northern Arizona, where the Colorado River becomes incised within the meanders of the Glen and Grand canyons, flowing through geological strata consisting primarily of sedimentary (sandstones, shales, and limestones) and metamorphic (schist and granites) material. The primary source of water for the Colorado River, in Grand Canyon originates now as a hypolimnetic discharge from Lake Powell Reservoir, at Glen Canyon Dam (0.0 km). The river descends 700 m in elevation from the dam to Lake Mead a total distance of 472 km. Sample site locations are relative to downstream distances (km) from Glen Canyon Dam, Fig 1.

Equipment and Data Collection

Three river trips were conducted in conjunction with two prescribed discharge tests (GCES-II 1990), May 20-30, 1991 at 425 m^3/s (15,000 ft^3/s); June 28-30 at 142 m^3/s (5,000 ft^3/s); and July 12-14 at 142 m^3/s (5,000 ft^3/s). The scheduled dates were selected for three reasons: 1) low probability of sediment contribution from tributaries; 2) constant discharge; and 3) ability to

differentiate volumetric differences in discharge for 142 and 425 m^3/s. Light attenuation measured at a specific discharge were not collected at all sites simultaneously, therefore, it can be assumed that these irradiametric measurements are sure to have been influenced to some degree by the antecedent conditions prior to or during each test flow.

Irradiametric measurements were collected using a series of underwater sensors (LiCor, Inc., Lincoln, Nebraska). Sensor types consisted of a spherical sensor (LI-193SA) collecting omni-directional or scalar irradiance. Two cosine corrected quanta sensors (LI-192SA) were deployed at a 180° vertical orientation for measuring downward irradiance and upward reflected irradiance. A terrestrial (LI-190SA) quanta sensor was used for measuring incidental surface measurements of solar radiation. Each type of sensor measured the spectral region between 400-700 nm with equal sensitivity. A compatible data-logger (LI-1000) with multiple channel capabilities, collected and stored irradiant measurements. Irradiant units of measure are expressed in microeinsteins m^2/s, μE. One μE is equivalent to 6.02×10^{17} quanta/photon.

Adjustment for the immersion effect was accomplished using the appropriate multiplier specific to each photosensors air-water calibration setting (Roemer and Hoagland, 1979; Kirk, 1983). To avoid refractive problems, surface based measurements were collected at 0.025 and 0.07 m depths respectively for cosine corrected and scalar quanta sensors. Irradiance was measured within a 45° solar declination to account for reflectant loss by water surface. Research indicates that vertical attenuation coefficients are not overly influenced by daily shifts within this solar angle of incidence (Kirk 1977). For this reason measurements were restricted between 0900 and 1530 hr in order to minimize reflectant loss to $\leq$ 2.8% of the available solar radiation (Kirk 1983). To avoid hysteresis a 10 s sampling time allowed for sensor equilibration between depth adjustment. Selection criteria was established to bracket underwater irradiance simultaneously with measured incidental solar radiation. Profile measurements for underwater depth irradiance were clustered to

within a 15% range of the solar incidence to avoid problems associated with irradiant flux due to changes in atmospheric conditions.

Figure 1 - The sampling site locations are numerically indicated for each irradiametric site conducted in the Colorado River, Glen and Grand Canyons.

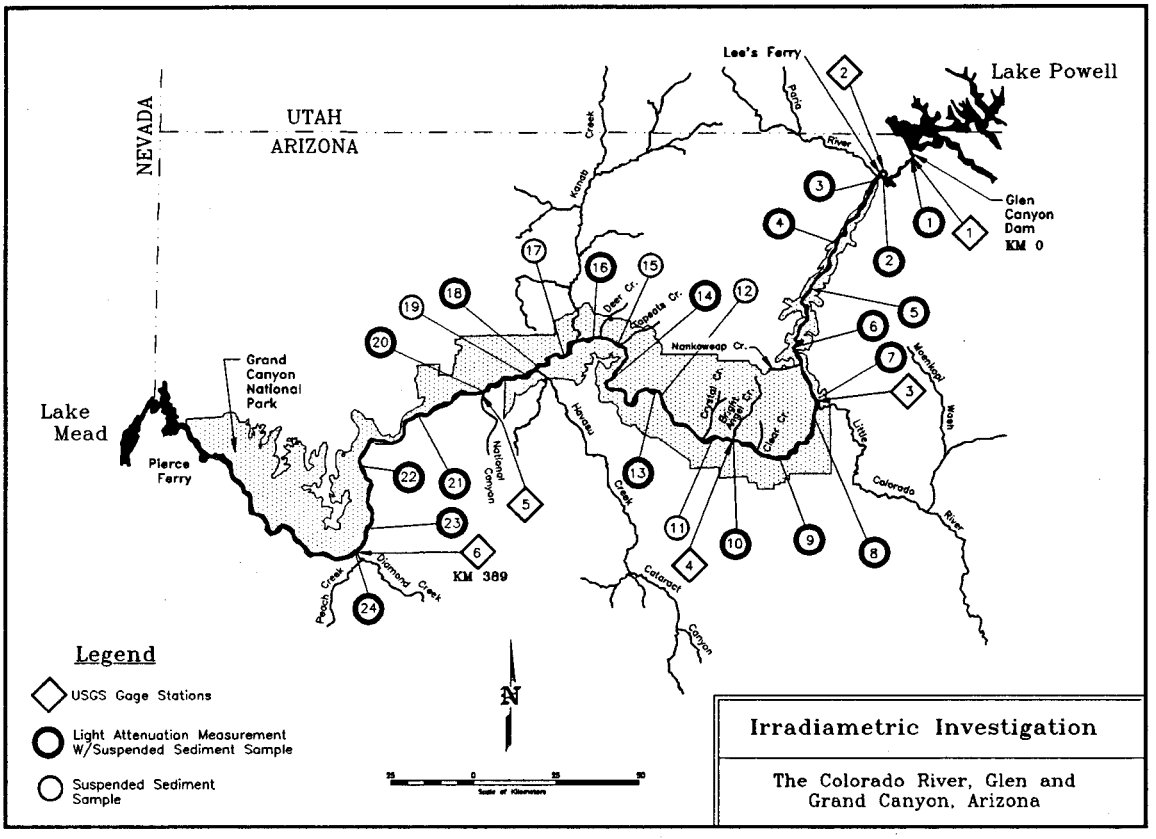

Sensors were mounted independently on a frame consisting of multiple support arms constructed in such a fashion that all depth intervals were identical to each sensor type (Fig. 1.2). All light measurements were collected simultaneously and related to a specific depth. Sensor types were lowered operating a pulley system connected to a suspension boom over the sun-ward side of the boat. Measurements were collected at 0.5 m depth intervals in direct sunlight when weather permitted.

Figure 2 - Deployment frame used for collecting depth integrated measurements for cosine corrected and scalar irradiance. Each sensor type is positioned to collect simultaneous measurements for a specific depth. The cosine corrected sensors are vertically oriented to measure downward irradiance, E_d , and upward reflectance, E_u . Scalar irradiance, E_o , is an omni-directional measurement (360°).

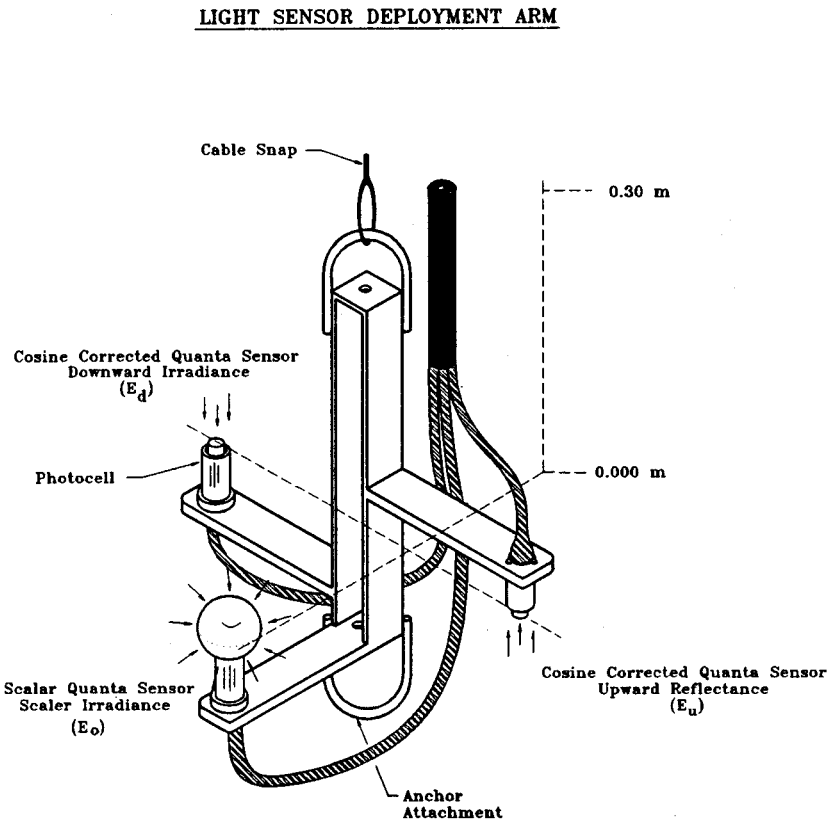

Depth integrated samples for suspended sediment were collected at each site using U.S. Geological Survey's sediment sampling techniques. Sampling equipment consisted of a D-77 sampler mounted on a bridge boom. It was assumed that at a constant discharge an integrated depth sample of suspended sediment concentration and particle size distribution was representative of the cross sectional stream flow (Pemberton 1987; Einstein 1950). Three integrated samples were collected in midchannel along the thalweg for each irradiametric site. All samples were stored, transported and analyzed for particulates, ash free dry weight (AFDW) and sediment. Weights were obtained using glass filters (Whatman 934-AH 1.5 μm pore size). Samples were desiccated for 1 hr. at 60°C, weighed ($\pm$ 0.0001 g), and ashed for 3 hr. at 550°C, and reweighed (Guy

1969). The three samples collected per site were converted to a mean concentration (g/L) for particulates, particulate organic matter (POM), and sediment. These concentrations were analyzed against the calculated light attenuation coefficient for each sample site.

A Hach, Inc., turbidimeter (model 16800), was used to measure turbidity from each integrated sediment sample. Samples were measured in nephelometric turbidity units, T_n, defined as a 90° scattering of light by suspended particulates (Kirk 1980a; Kirk 1980b). Water quality data were collected using a Hydrolab Inc., DS2H, including temperature (°C), pH, conductivity (μmhos/cm^2), and dissolved oxygen (mg/L). A secchi disc was used to collect depth measurements in conjunction with irradiametric measurements at the same sample site.

Data Analysis

Photosynthetically available radiation, *PAR* , exponentially declines with depth (Kirk 1983; Williams *et al.* 1980). Light attenuation in water results from the combined effect of the physical components which scatter and ultimately absorb light, these include; water, soluble dyes (i.e. water-soluble humic substances), and suspended organic and inorganic material (Kirk 1977; Kirk 1983). Kirk (1977; 1980a; 1983) identified that the presence of inorganic and organic particulates are at times major factors in light attenuation for some natural bodies of water. The vertical attenuation coefficient, K , was used to characterize the Colorado River's light impeding properties as a function of discharge downstream from Glen Canyon Dam. This parameter allowed us to spatially characterize the availability of *PAR* as optical characteristics of the river system changed longitudinally with increasing distance from Glen Canyon Dam.

The exponential attenuation of *PAR* is linearized using eqn. 1, which is a natural log transformation of irradiance at a specific depth. The vertical attenuation coefficient is calculated

$$\ln Q = - Kz + \ln Q_o \quad (1)$$

using an equation developed by Kirk (1977; and 1983) which is a derivative of eqn. 2,

$$Q = Q_o e^{-Kz} \quad (2)$$

Refer to Appendix B, for additional information concerning methods used in calculating coefficients for vertical attenuation, absorptance, and scattering.

Optimum light conditions in the Colorado River for photosynthesis are best described as a relationship of depth where the compensation point of C. glomerata exceeds the channels mean thalweg depth. Under sub-optimum light conditions, channel depths exceed available light. Photosynthetic intensities (μE) specific to C. glomerata were derived from previous research findings (Mantai 1974; Graham *et al.* 1982). As identified by Graham *et al.* (1982), the measured compensation point for C. glomerata extended from 25 to 35 μE for water temperatures ranging from 5°C to 20°C. A mean intensity value of 30 μE was selected as the compensation point for calculating Z_{cp} at variable incidental surface intensities rather then determining Z_{eu} from 1% *PAR*. Differences in saturation levels identified for Cladophora spp. vary between 920 μE (Mantai, 1974), and 345 to 1125 μE (Lester *et al.* 1974). Mantai (1974) reported that the point of photosynthetic saturation did not occur at low light intensities. We selected the depth of the saturation point based on the findings of Mantai (1974). The vertical zone for maximum net photosynthesis was calculated using a range in intensities from 300 to 600 μE for each site (Graham *et al.* 1982).

The compensation depth was calculated using K the attenuating slope of subsurface light and the mean incidental light intensity measured during the depth profile by solving for the line-intercept. The equation (eqn. 3) below is used for determining the depth of the compensation point;

$$Z = -1\ /K \cdot \ln I + 1\ /K \cdot \ln I_{ss} \quad (3)$$

The derivative, eqn. 4, uses the constant 3.4 which is natural log transformation of the irradiant intensity identified as the compensation point, 30 μE for C. glomerata (Graham 1982).

$$Z_{\text{compensation point}} = 3.4 - \ln I\ /\ K \quad (4)$$

The constant (3.4) is specific to C. glomerata or other aquatic algae sharing similar compensation points and should be used as a relative base of measure if mean values of incidental light intensity are collected in conjunction with attenuation data (refer to Appendix B).

The sampling approach allowed us to characterize the optical properties of the Colorado River by stratifying the river longitudinally into irradiametric reaches. Sampling site locations were designated at 25 kilometer intervals, including specific sites located at major tributaries and the USGS gage stations. A total of 24 sites were sampled for suspended sediment concentration, and of these, 19 sites were correlated with irradiametric measurements. Locations of sampling sites on the Colorado River are indicated in Fig 1. This is an area that extends from Glen Canyon Dam to Diamond Creek, a distance of 387 km downstream.

Mean thalweg depths, velocities, channel slope and channel width for each designated reach were derived from data compiled from USGS bed material maps as part of the Sediment Transport and River Simulation (STARS) model (Randel and Pemberton 1987). The mean thalweg depth, channel slope and channel width were adjusted to reflect changes in vertical stage for discharges of 142 and 425 m^3/s. For purposes of comparing geomorphology sampling sites were converted into 19 irradiametric reaches. The designated reach lengths were either half the distance between adjacent sites both upstream and downstream, or demarcated at the confluence point of the primary

tributaries (Paria River, Little Colorado River, and Kanab Creek). The calculated attenuation coefficient for each sample site is representative of this longitudinal distance. These hydraulic and geomorphological variables represent the channel characteristics for each of the designated irradiametric reaches. We compared this to 11 geomorphic reaches previously delineated by Graf *et al.* (1989), which represented general differences in the hydraulic characteristics and sedimentary features of the Colorado River. Our sample sites were overlaid with these distinct areas to determine if a relationship existed between geomorphology and vertical light attenuation. The channel geometry data were derived from the same source, however, the reach designations and flow discharges (682 m^3/s) evaluated were different. For additional information regarding the hydrological characteristics of Grand Canyon reaches refer to Graf *et al.* (1989).

RESULTS

Analysis of Vertical Light Attenuation

The irradiametric data for the two evaluated discharges, 142 and 425 m^3/s, were analyzed separately. It was identified that vertical attenuation coefficients for scalar irradiance are positively correlated to sediment concentration, distance and discharge from Glen Canyon Dam. Each of these factors demonstrated a positive correlation to light attenuation and are listed in order of greatest significance.

Sediment Concentration effects on Attenuation of PAR

Concentration levels of suspended sediment varied at sites replicated at different discharges measured at 142 and 425 m^3/s, (Fig. 3 and 4). The results from our analysis identified that light attenuation coefficients (K_o) were significantly correlated to particulates (i.e. this includes sediment and organic matter) at only the higher discharge 425 m^3/s ($F_{1,18} = 42.432$, $R^2_{adj} = 0.686$, $p < 0.0001$); however, no significance was found to exist at the lower discharge 142 m^3/s. It was

Figure 3 – Concentration of suspended sediment (g/L) at discharge of 142 m^3/s. The mean concentration value is plotted against distance (km) from Glen Canyon Dam. The standart error in sediment concentration for each site is represented by the error bar.

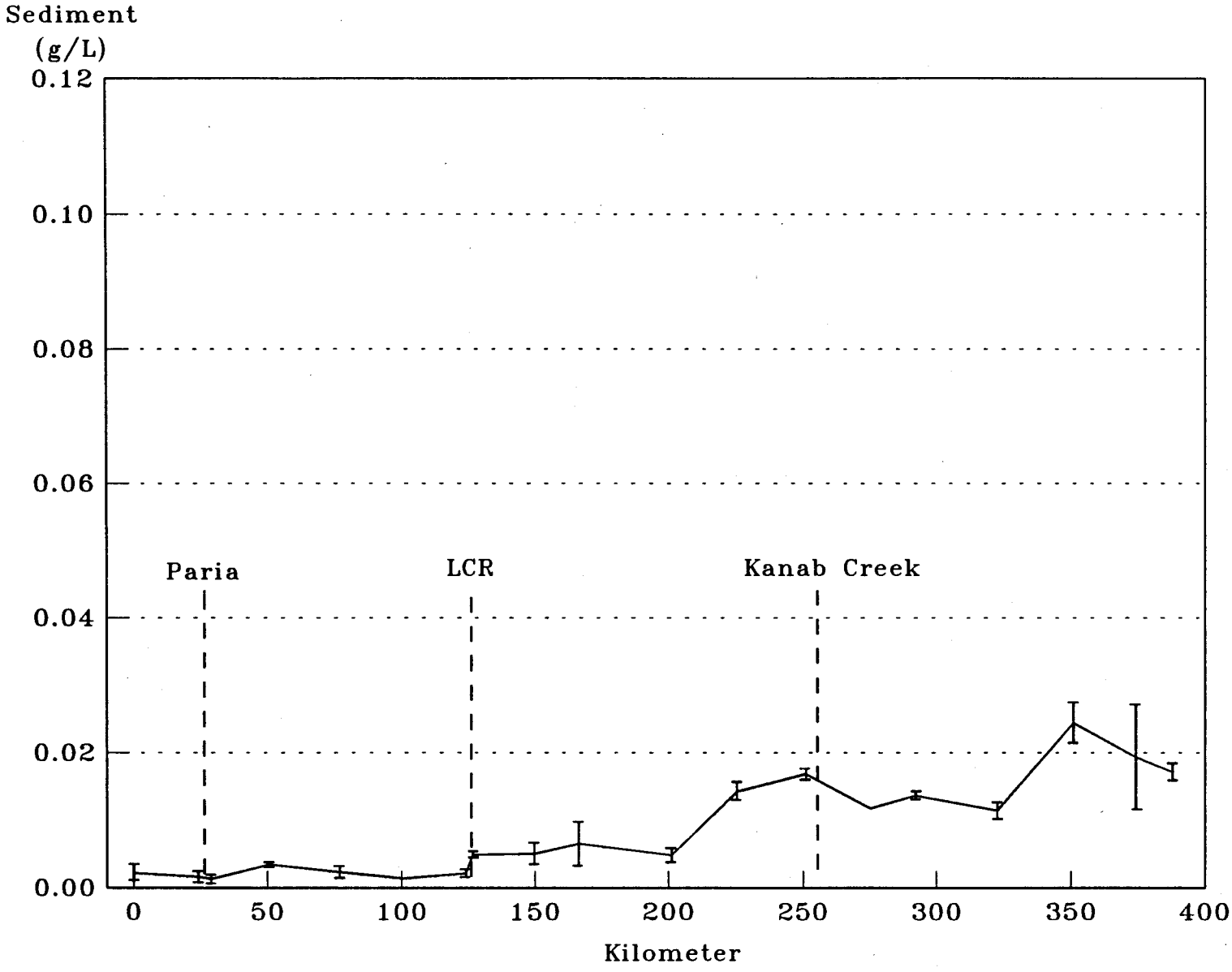

Figure 4 – Concentration of suspended sediment (g/L) at discharge of 425 m^3/s. The mean concentration value is plotted against distance (km) from Glen Canyon Dam. The standard error in sediment concentration for each site is represented by the error bar.

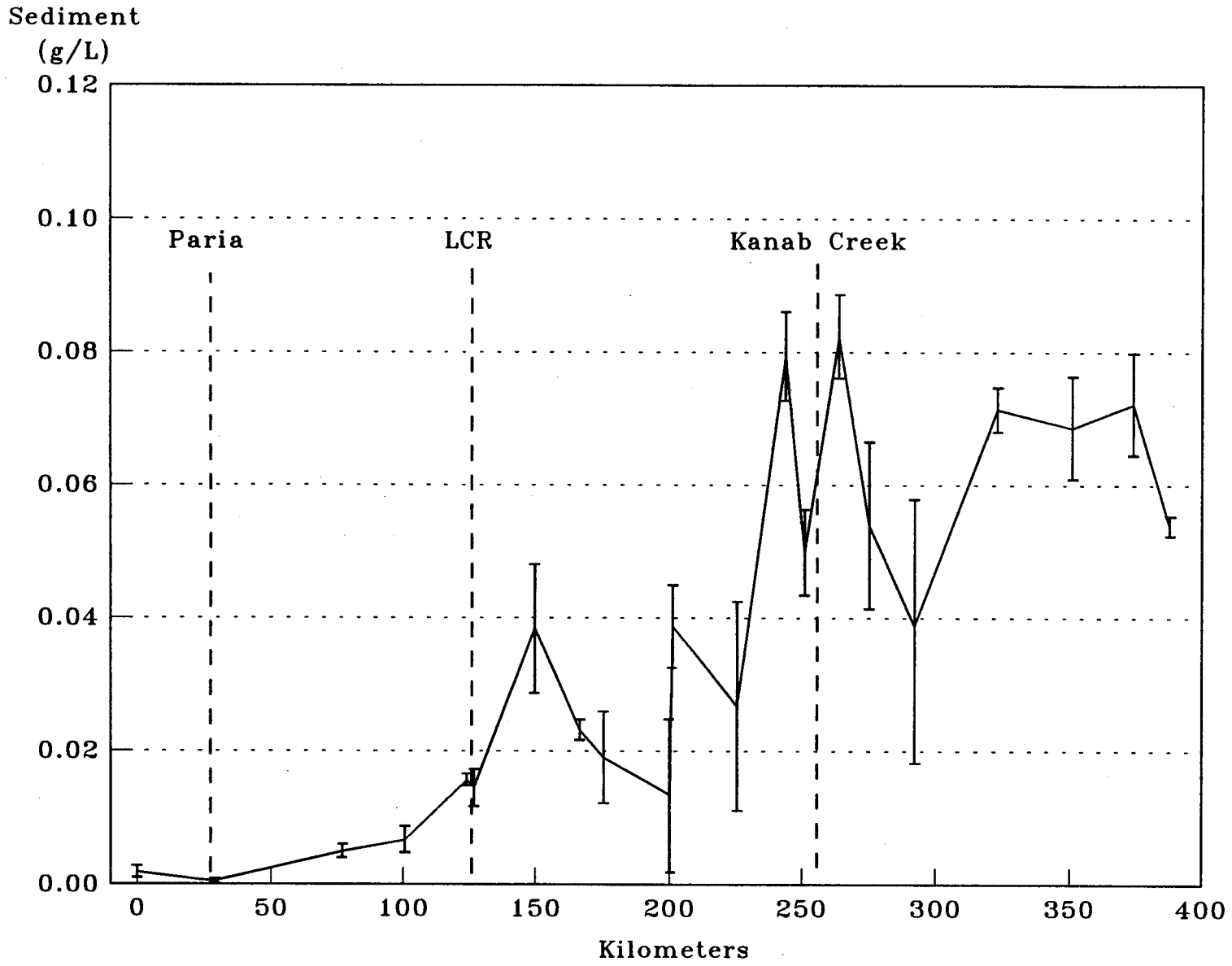

found that the fraction consisting of particulate organic matter (POM) collected as part of the integrated sample obfuscated our results. POM concentration was found not to be significantly correlated to light attenuation for either of the two discharges. The removal of organic particulates disclosed that light attenuation was significantly effected by sediment concentration at both discharges. The ANOVA's conducted on attenuation coefficients for scalar irradiance indicated a positive correlation between light attenuation and sediment concentration. The results for each discharge measured were significant ($F_{1,18} = 42.432$, $R^2_{adj} = 0.686$, $p < 0.0001$) at 142 m^3/s, and ($F_{1,17} = 75.192$, $R^2_{adj} = 0.805$, $p < 0.0001$) at 425 m^3/s. Elevated levels of suspended sediment were related to volumetric increases in discharge from Glen Canyon Dam as a result of accumulation in sediment load. The empirical data collected for sediment concentrations verifies the light attenuation data found in Table 1 and 2 (Appendix A).

The vertical attenuation coefficient, K_o , for scalar irradiance can be derived using data collected on mean sediment concentrations. The two developed regression equations for light attenuation are based on the compilation of mean sediment concentration data collected for all sites. The regression equations for calculating attenuation coefficients from variable sediment concentrations are identified: 1), for 142 m^3/s discharge (eqn. 5);

$$K_o = 17.896 \cdot Q_s + 0.291 \quad (R^2_{adj} = 0.686) \tag{5}$$

and 2), for 425 m^3/s discharge (eqn. 6).

$$K_o = 11.945 \cdot Q_s + 0.317 \quad (R^2_{adj} = 0.805) \tag{6}$$

The above results indicate a linear relationship between concentration and light attenuation for both regressions. The linear regressions were tested (students-t) to determine if significant differences

existed between the two calculated slopes. The findings indicate that both linear regressions are equivalent ($t_{0.05}$ (2), 35 = -0.057). Refer to Fig 5, for a graphic representation of the combined data set (n=38) for both discharges. This graph demonstrates the linear relationship between vertical attenuation coefficients, K_o , and mean concentration of suspended sediment, Q_s . It appears that at this juncture, with the limited range of samples available that attenuation of light is a linear function to sediment concentration. However, from our analysis, the assumption that a linear relationship exists between sediment concentration and light attenuation over a wide range of sediment loads from discharges or tributaries in the Colorado River cannot be verified.

Distance effects on the Attenuation of PAR

As identified, distinct changes in light attenuation resulted with increasing distances downstream from Glen Canyon Dam. In evaluating light attenuation to increasing distances a positive correlation was observed to be significant regardless of the actual discharge volume. The results are listed respectively for discharges measured at 142 m^3/s ($F_{1,18}$ = 150.551 , $p < 0.001$, R^2_{adj} = 0.887), and 425 m^3/s ($F_{1,17}$ = 59.103, R^2_{adj} = 0.763, $p < .001$). Refer to Fig 6, demonstrating a positive correlation between light attenuation and distance at discharges measured at 142 and 425 m^3/s.

Vertical attenuation coefficients, K_o , were converted to percent light attenuation for the purposes of sample site comparison. The K_{avg}, for Glen Canyon Dam represents the percent baseline (0%) for light attenuation in the Colorado River. The mean calculated attenuation coefficient, K_{avg} , at the base of Glen Canyon Dam (0 km) during the summer period for scalar irradiance was 0.238 ± 0.016 (s.d.) at discharges of 142 and 425 m^3/s. This narrow range between attenuation coefficients is indicative of an optically stable source of water originating from Glen Canyon Dam within the discharge range evaluated during this experimental period. Differences in percent increase in light attenuation downstream from Glen Canyon Dam are based

Figure 5 – The two regressions are equivalent and graphically demonstrate the linear relationship between vertical attenuation coefficients for scalar irradiance, K_o, and mean concentration (g/L) of suspended sediment, Q_s.

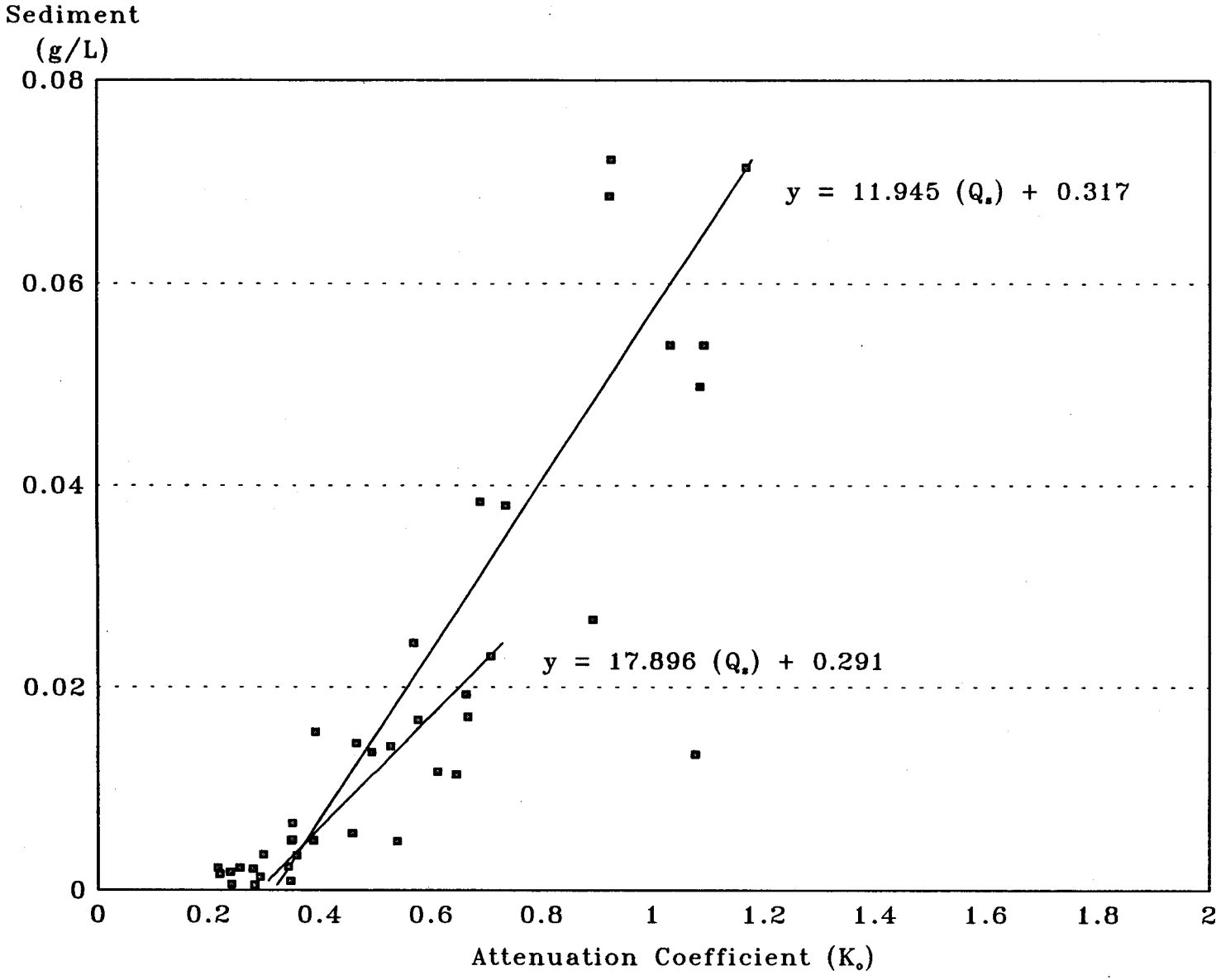

Figure 6 – Vertical attenuation coefficients, (K_o), for scalar irradiance measured at two steady state discharges of 142 m^3/s and 425 m^3/s on the Colorado River from Glen Canyon Dam (0 km) to Diamond Creek (387 km).

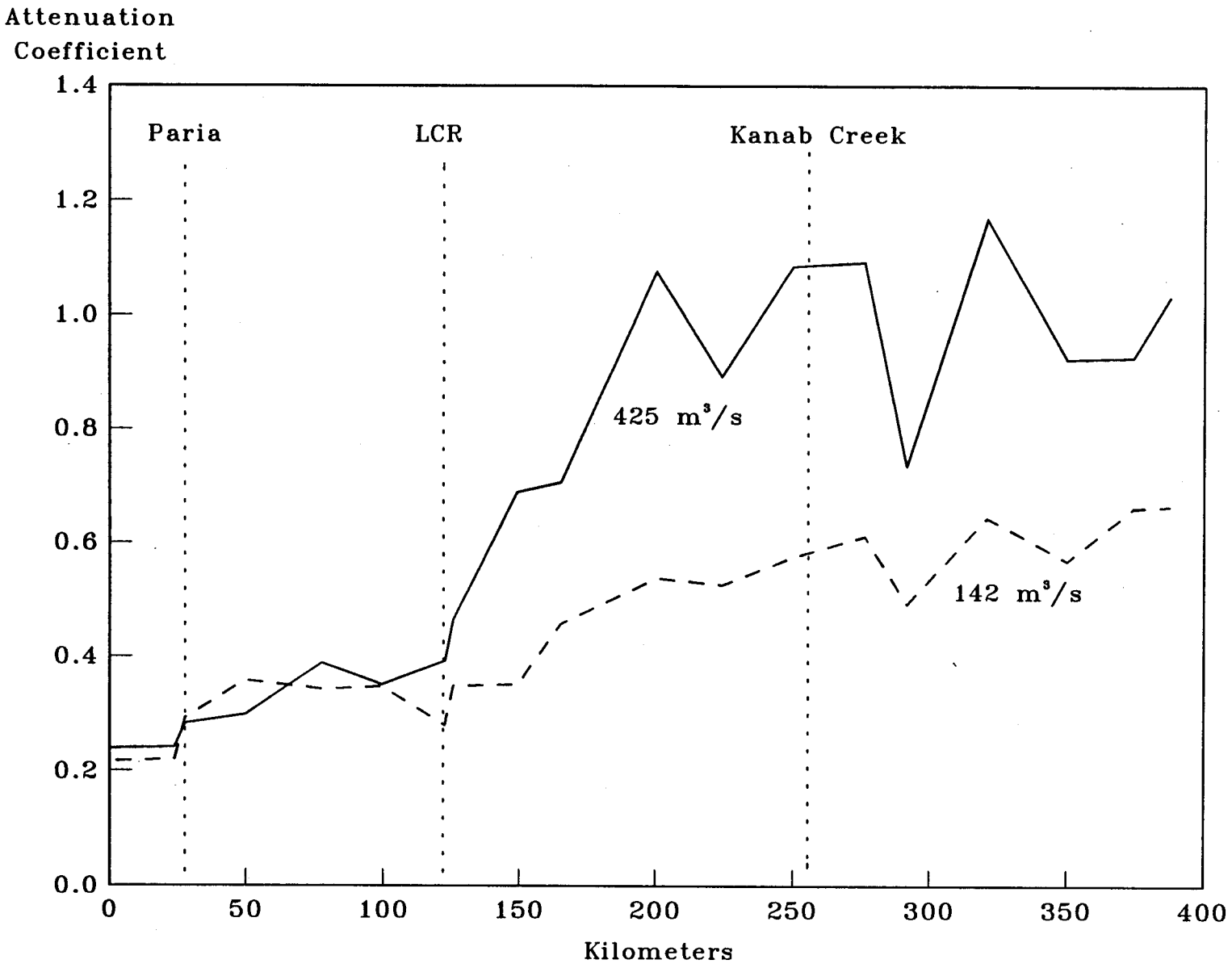

on the percent change from Glen Canyon's K_{avg} coefficient value. Percent change in light attenuation increased from Glen Canyon Dam to Diamond Creek a distance of 387 km. At Diamond Creek the maximum percent change in light attenuation varied from 180% (142 m^3/s) to 335% (425 m^2/s). This indicates that the differences in discharge volume influence the sediment transport capacity (Cluer 1992), and ultimately *PAR* by almost an order in magnitude. Also, percent change in vertical light attenuation with increasing distances downstream responded similar in pattern to the delineated hydraulic reaches of the Grand Canyon (Graf *et al.*, 1989).

It became apparent that the significance of distance (KM) as a variable effecting light attenuation was not independent of a combination of other interacting variables. In evaluating this phenomena, independent of the effect of discharge, we attributed the differences in light attenuation with increasing distances downstream to three factors; sediment carrying capacities, unique hydraulics and channel geomorphology of the Colorado River. At a constant discharge, the variation observed downstream in light attenuation were tested against the geomorphological changes in mean channel width, depth, and slope using a multiple stepwise procedure. In using a Pearson's correlation matrix on the collected and interpolated data developed from the Stars simulation model, we found no correlation between depth and slope with light attenuation. The only geomorphological variable that was found to be correlated to light attenuation was channel width, but only at a discharge of 425 m^3/s. An ANOVA showed that a negative correlation for channel width to light attenuation was significant ($F_{1,15} = 7.166$, $R^2_{adj} = 0.278$, $p = 0.017$). The other geomorphic variables representing depth and slope appear not to significantly explain the response of increased light attenuation with increasing distances.

Light Absorptance and Scattering

Light attenuation is the direct result from the effects of both the absorptive and scattering characteristics of the constituents within the water column. Due to sampling difficulties

absorptance coefficients were derived only for a discharge of 142 m^3/s. In analyzing the relationship of sediment to light absorptance it was determined that sediment was a significant factor ($F_{1,18} = 41.931$, $R^2_{adj} = 0.683$, $p < 0.001$). In the Glen Canyon reach, light attenuation is minimal ($K_{avg} = 0.238$). Within this reach coefficient ratios of light absorptance, (*a*), to vertical attenuation, *K* , indicate that absorptance accounts for a higher proportion of the overall light attenuation, 71% ± 0.08 (s.d.). A distinct shift in light absorptance occurs below the Paria River at Site 3 (28 km). The shift in *a/K* ratios below the Paria tributary indicates that scattering becomes nearly equivalent to light absorptance in the overall aspect of light attenuation. The ratio of *a/K* remains fairly proportional at 55% ± 0.05 (s.d.) for the remainder of the study area approximately 360 km, even though light attenuation for downward and scalar irradiance continues to increase downstream. It is speculated that the shift in *a/K* ratios are due to a change in optical characteristics below the Paria tributary as a result of the combined effect from light absorptance and scattering by sediment. Whereas, absorptance in the Glen Canyon Reach results from primarily water, organic particulates and dissolved dyes originating from Lake Powell reservoir. The light absorptance from these components becomes dominated by the overriding presence of sediment from the Paria downstream to Diamond Creek. Sediment accounts for the greatest aspect of light absorbance, and is graphically represented in Fig 7.

Total scattering (*b*) increases with distance downstream from Glen Canyon Dam. The varying values for scattering coefficients for the same site represent differences due to discharge volume indicating that scattering further increases light attenuation. The increased levels of suspended sediment disrupt the vertical orientation and directional path of light, further increasing the light scattering aspect of the water. Light scattering becomes very pronounced under higher discharges and in geomorphic reaches having higher turbulence. An ANOVA conducted showed significance ($F_{1,8} = 6.089$, $R^2_{adj} = 0.361$, $p = 0.039$) of sediment concentration to light scattering, with a positive trend. The absorptance and scattering properties of each site are presented in

Figure 7 – Absorptance coefficient, a, for the Colorado River at a discharge of 142 m^3/s. Absorptance coefficients were calculated at an optical depth of 2.3 = Z_m, representing 10 % of total PAR. The standard error represents the absorptance coefficient measured for the entire depth profile.

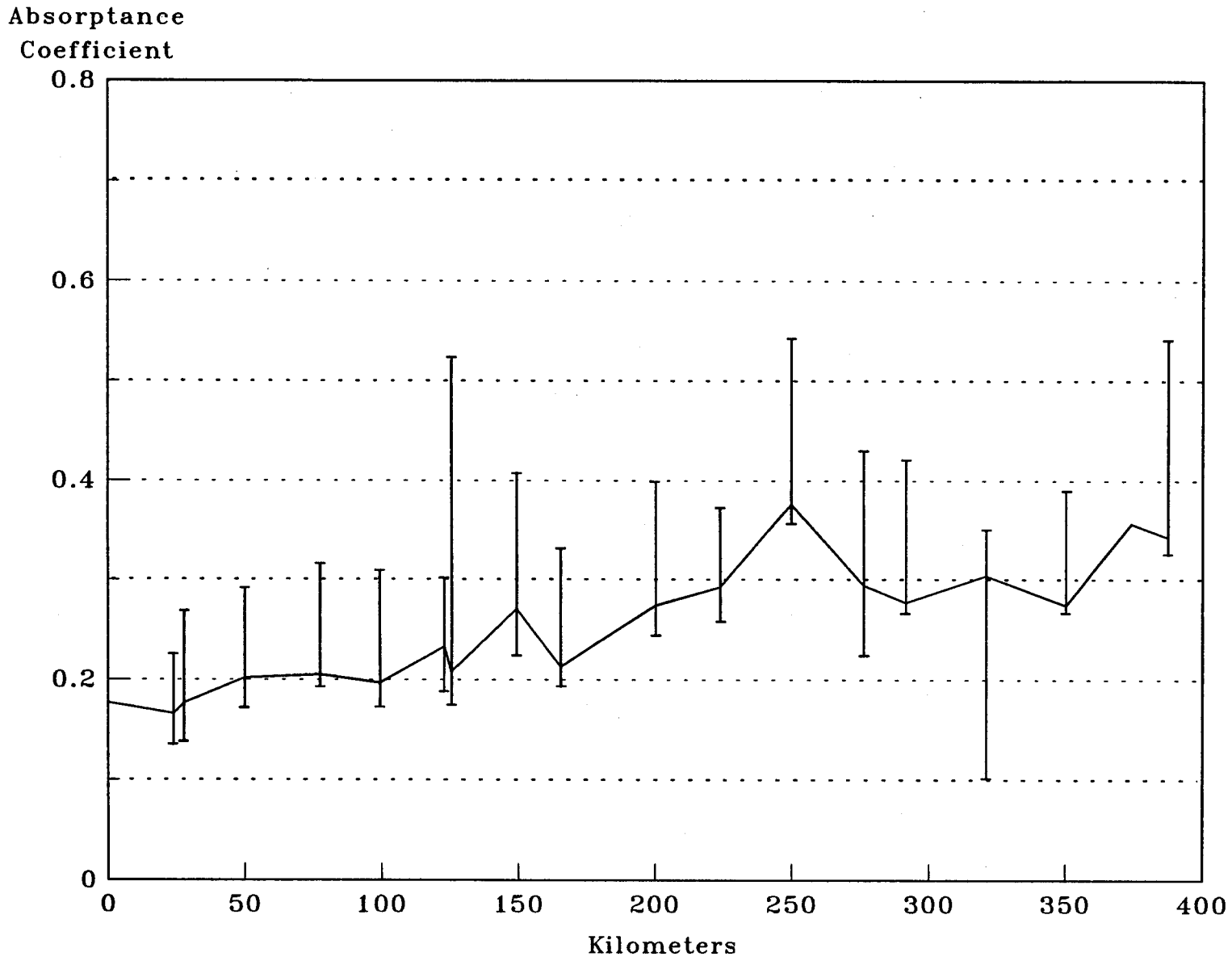

Tables 3 and 4 (Appendix A), listing coefficient values for vertical attenuation, K , asymptotic reflectance, R_a , asymptotic backscattering, b'_b , normal backscattering, b_b , and total scattering coefficient, b , for discharges of 142 and 425 m^3/s. Nephelometric turbidity, T_n , and the ratios between asymptotic backscattering and normal backscattering coefficients are also listed.

The correlation coefficient, R^2 , between asymptotic backscattering, b'_b , and turbidity, T_n , for all measurable sample sites at both discharges was 0.943 . The mean ratio for T_n to b'_b was 32.5 ± 4.9 (s.d.) in waters of varying turbidity. This reconfirms Kirks (1980a) research which produced a similar mean ratio value of 30.6 ± 4.8 (s.d.) indicating that there is a linear relationship to asymptotic backscattering and turbidity (Fig 8). The asymptotic backscattering coefficient can be derived from nephelometric turbidity, T_n , applying eqn. 7.

$$b'_b = 0.336 \cdot T_n - 0.00722 \text{ , } (R^2 = 0.943) \qquad (7)$$

It was not possible to identify the asymptotic reflectance at all sites and discharge levels due to the affects of channel bed reflectance. In addition, R_a , was not encountered at certain sites because of profile depths in waters having a low K_d value.

Optical Light Conditions (μE) within the Colorado River's Euphotic Zone

The optical light conditions are defined by the underwater light regime relative to the compensation point for C. glomerata to the channels mean thalweg depth. Data generated from the STARS simulation model was reanalyzed to determine the effect of vertical change in stage on light availability. Our results indicate that for a volumetric change in discharge from 142 to 425 m^3/s from Glen Canyon Dam to Diamond Creek results in an overall change in mean vertical stage of 1.68 m ± 0.55 (s.d.), (n = 707). Table 5 and 6, lists mean thalweg depths, widths, slope, velocity, and compensation point and percent light availability for each site. The mean depth for

Figure 8 – Asymptotic backscattering coefficient, (b'_b), to nephelometric turbidity units (NTU).

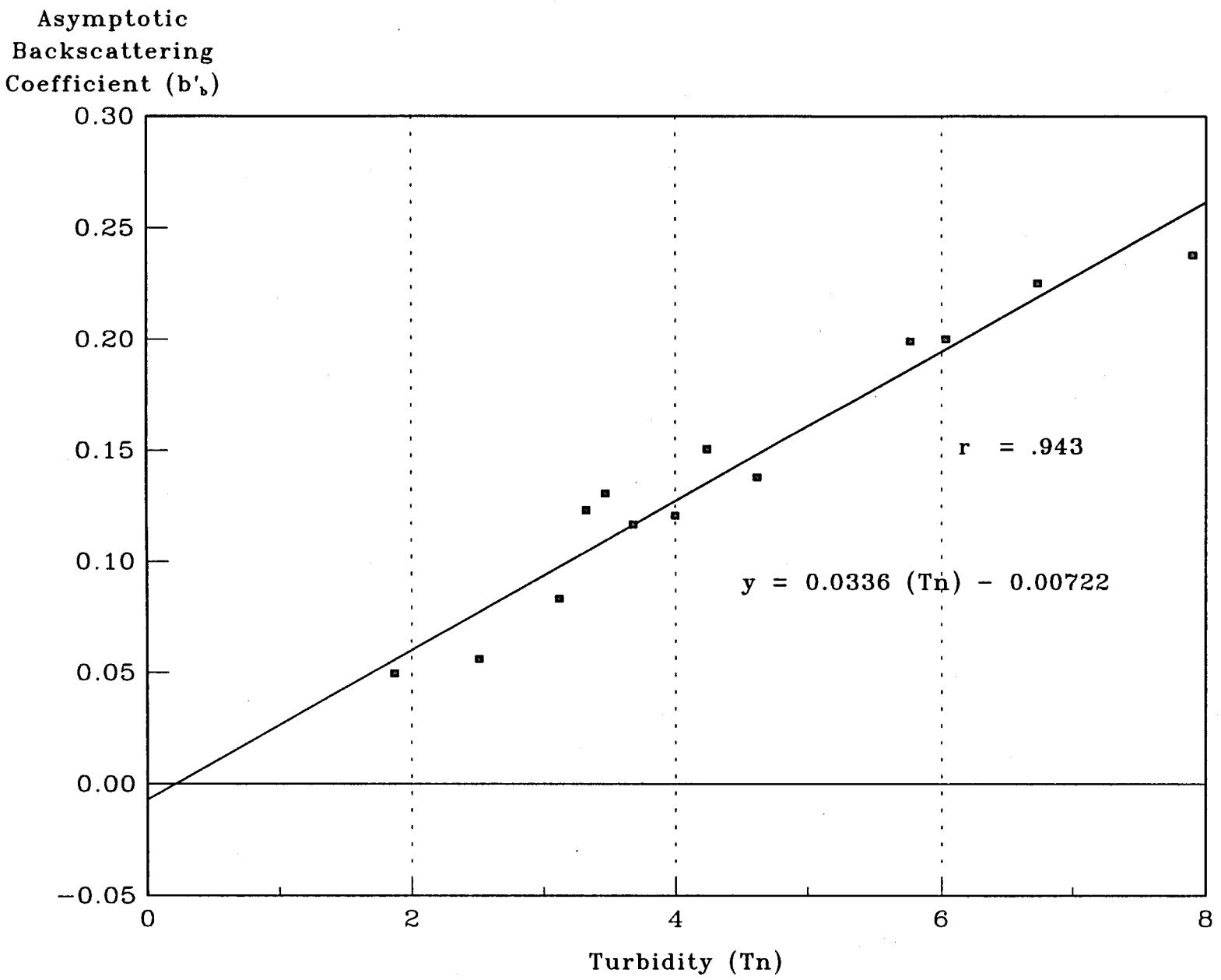

142 m^3/s is 5.26 ± 4.13; and 425 m^3/s is 6.95 ± 4.32. The depths were adjusted to reflect differences in depth at these discharges and are representative of each irradiametric reach.

At a constant discharge of 142 m^3/s the mean thalweg depth does not exceed the compensation point for C. glomerata for the entire extent of the Colorado River. Whereas, at a higher discharge (425 m^3/s) sub-optimum light conditions predominate, restricting the compensation point (30 μE) and the potential use of the channel bed to shallower depths for a large portion of Grand Canyon. The available area for algal growth will be reduced from the upper portion of the Granite Gorge (150 km) to Diamond Creek (387 km) at discharges of 425 m^3/s or greater. At this discharge the mean thalweg depth exceeds the Z_{cp} , resulting in a 25 to 50 percent loss of the lower vertical zone of the channel. These reaches are subjected to photosynthetic exclusion or temporary concealment due to increased light attenuation. The increase in wetted perimeter resulting from a higher discharge (425 m^3/s) will not compensate for the reduced photosynthetic zone in reaches of the middle and lower Grand Canyon due to increases in light attenuation. And yet, the optimum photosynthetically available light will exist from Glen Canyon to Little Colorado River under both discharges regimes at 142 and 425 m^3/s. However, even though these optimum light conditions are available in the Marble Canyon and Lees Ferry reaches, the quantity in percent of total *PAR* will be appreciably reduced in irradiant intensity. Refer to Table 7 and 8 (Appendix A), for changes in percent change in total *PAR* .

Tables 7 and 8 (Appendix A), identify depths for observed and calculated Z_{cp} at flow discharges of 142 and 425 m^3/s. The calculated depths for the compensation point, Z_{cp} , maximum net photosynthetic range (300-600 μE), and the saturation point Z_{cp} are graphically represented in Fig 9 and 10. The zone of maximum net photosynthesis (300-600 μE) is reduced from Glen Canyon to Diamond Creek at both discharges for the extent of the Colorado River.

Figure 9 : Longitudinal distribution of light attenuation in the Colorado River at a 142. m^3/s discharge. Derived depths (m) for subsurface intensities are specific to C. glomerata, from research identifying compensation point (Z_{cp}), net photosynthesis (Graham *et al*. 1982), and saturation point (Mantai 1974). Mean channel depths have been adjusted to actual stage elevation (Randel and Pemberton 1989).

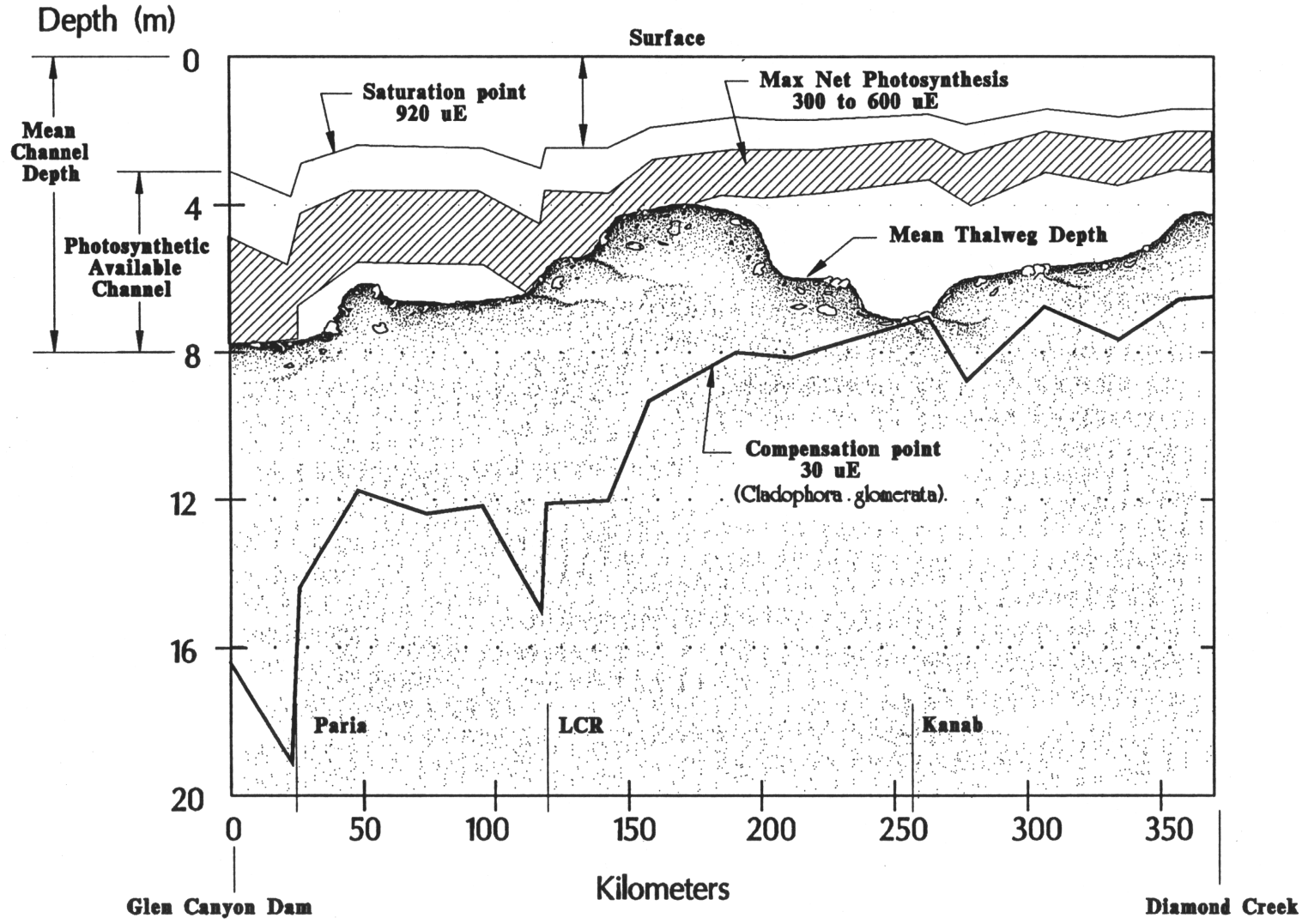

Figure 10 : Longitudinal distribution of light attenuation in the Colorado River at a 425 m^3/s discharge. Derived depths (m) for subsurface intensities are specific to C. glomerata, from research identifying compensation point (Z_{cp}), net photosynthesis (Graham *et al*. 1982), and saturation point (Mantai 1974). Mean channel depths have been adjusted to actual stage elevation (Randel and Pemberton 1989).

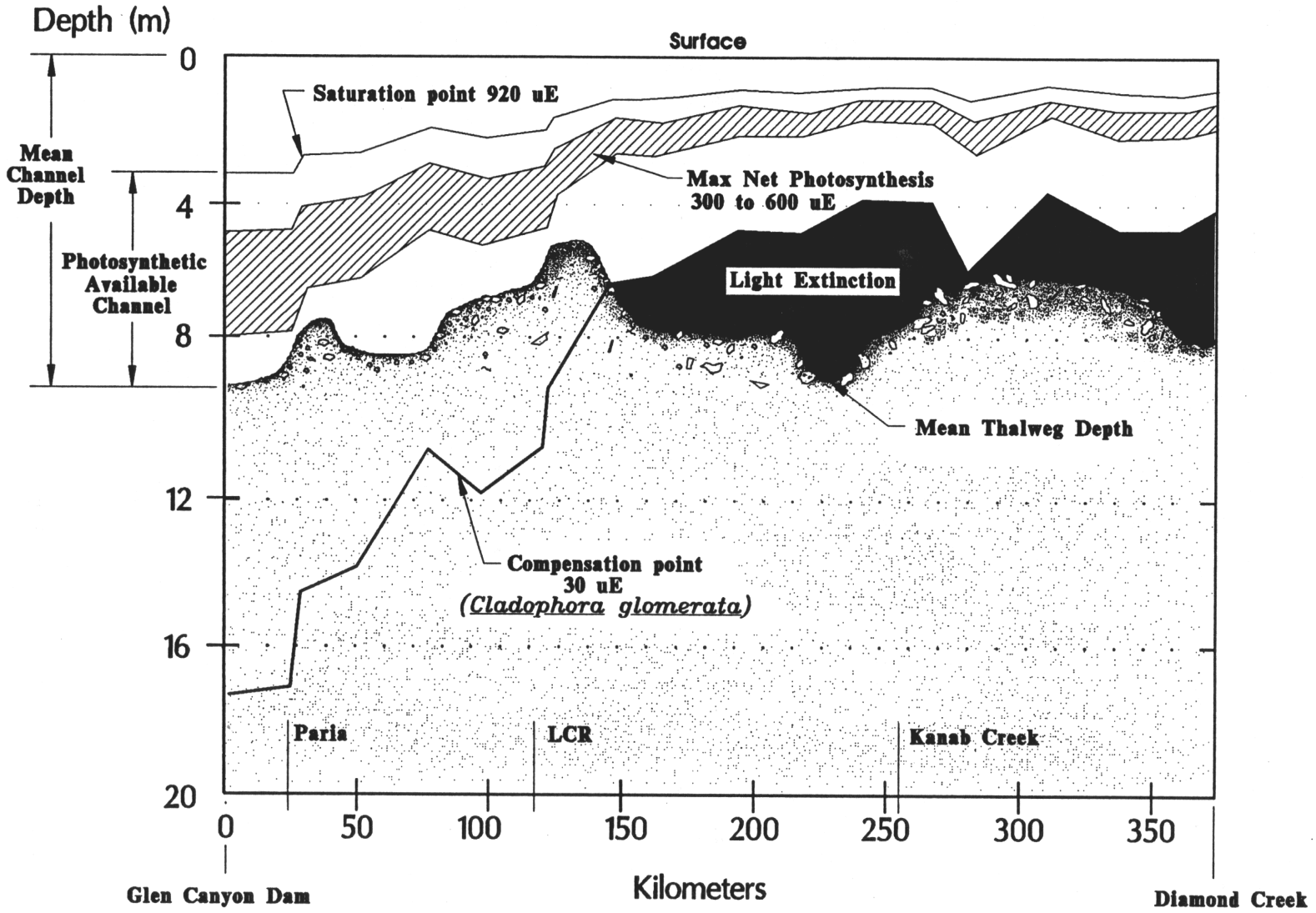

Light attenuation measured in the Glen Canyon area had similar attenuation coefficients under two constant discharges measured at 142 and 425 m^3/s, refer to Tables 1 and 2 (Appendix A). However, on July 11, 1991, irradiametric measurements collected during fluctuating flow conditions for scalar irradiance showed an elevated attenuation coefficient of 0.302 (R^2 = 0.990) at a discharge level ranging from 736 m^3/s to 793 m^3/s (refer to the analysis section in Appendix C). Irradiametric measurements collected the following day at a constant discharge of 142 m^3/s displayed reduced attenuation coefficient, K_o , of 0.220 , (R^2 = 0.996), which were similar to those previously measured attenuation coefficients for discharge levels at 142 and 425 m^3/s. This indicates that discharges in excess of 425 m^3/s have a disrupting effect on the stability of the underwater light regime as previously observed in the Glen Canyon area. Additional data has not been collected under conditions of fluctuating flows for other portions of the Colorado River downstream in Grand Canyon.

DISCUSSION

Analysis of Vertical Light Attenuation

Aquatic productivity derived from photosynthesis is strongly influenced by the underwater light regime throughout the Colorado River. Growth of C. glomerata is exceedingly important to the Colorado River since it represents a major biological substrate for epiphytyic diatoms (Hardwick *et al.* 1992). Difficulties arise in assessing the primary factors that control distribution and growth of aquatic plants due to the numerous variables encountered in a river system (Spence *et al.* 1970; Jewson and Taylor 1978). Certain studies have identified limiting factors that affect the photosynthetic capabilities of aquatic algae; these have focused on temperature optimums (Hodgson 1981; Graham *et al.* 1982), desiccation (Usher *et al.* 1987; Hodgson 1981), light intensities (Graham 1982; Marcus 1980; Jones and Ilmavirta 1978; Grande *et al.* 1989; Adams and Stone 1973; Spence and Chrystal 1970) and spectral composition of light (Pantastico and Suayan 1973; and Larkum *et al.* 1966). Usher *et al.* (1987), identified trends of decreasing

biomass in C. glomerata with increasing distances from Glen Canyon Dam, and speculated that seasonal growth may either be regulated by light or nutrient levels in waters of relatively constant temperature. Our data indicate that in the Colorado River light availability will become a primary limiting factor in aquatic productivity under a discharge regime of 425 m^3/s or greater during periods of minimal concentration of sediment under tributary baseflow.

Sediment Concentration effects on the Attenuation of PAR

Our study has identified a relationship between light attenuation and sediment concentration under optimum water clarity conditions during periods of minimal tributary contribution. In other studies, methods used in correlating sediment concentrations to vertical light attenuation have not been entirely successful. This is partly attributed to the physical variability in particle size distribution, shape and refractive indices of the sediment (Spinrad 1978; Kirk 1980a). Also, it is speculated that our results showing a linear relationship are due to the removal of the particulate organic matter, since values for sediment concentrations generally do not account for this organic fraction.

Additional information exists on the effect of suspended sediment on light availability and its behavior (Kirk 1983; Jones and Wills 1956; Di Toro 1978; Duchrow Everhart 1971; and Scott 1978). The light attenuation regression (eqn. 6) provides researchers with an accurate estimator of light attenuation under a narrow range of sediment loads. Since the Colorado River can be extremely variable in sediment loads during periods of tributary influence our findings may not be applicable to correlating vertical light attenuation coefficients under excessive sediment concentrations ($\geq$ 0.0722 g/L). As it stands, the linear relationships shown in eqn. 5, and eqn. 6, are not an accurate model for predicting vertical light attenuation derived outside of the sediment concentration range of this investigation. This is primarily due to the extreme variability in concentration, particle size and refractive differences of sediment transported from dissimilar tributaries (Kirk 1983; Randel and Pemberton 1987; Herford 1984). Therefore, additional analysis

for irradiametric and sediment concentrations are required at variable discharges and periods of tributary input to determine whether or not a predictive model can be developed using sediment concentration data. This information is sure to be beneficial if sediment concentrations are to prove to be a reliable predictor of light availability in the Colorado River.

The significant interference from particulate organic matter must be taken into account before attempting to correlate light attenuation to low sediment concentrations. The overriding interference is not significant at higher sediment concentrations. Additionally, it is interesting that our mean values for POM at 142 m^3/s, 0.0081 ± 0.0012 g/L, n = 7; and at 425 m^3/s, 0.0038 ± 0.0009 g/L, n = 5, collected in the Glen Canyon Reach were considerably higher than the mean values (0.0006 ± 0.00004 g/L) observed by Angradi (1992). The discrepancies in our findings are probably related to methodological differences (i.e. Miller-tube and AFDW at 2 h. intervals), sampling time and size. It is important to note that POM was observed to increase with increasing distances downstream, (refer to Table 1 and 2). We contend that the increase in POM is in part related to the export of POM from the Glen Canyon Reach in addition to photosynthetic activity occurring downstream.

Distance Effects on the Attenuation of PAR

As identified, increases in volumetric discharge from Glen Canyon Dam of 142 to 425 m^3/s result in an overall increase in light attenuation by almost an order of two over a distance of 387 km. Reaches where channel gradients decrease in slope, light attenuation became reduced but not in proportion to other reaches of similar hydraulic and geomorphic characteristics observed further upstream.

Decreases in mean channel depths and widths may explain the abrupt or gradual shifts observed in light attenuation at distinct sites or broad geographical areas. The reduction in channel depth can

resuspend sediment by increasing turbulence (Colby 1961); whereas, wide channel widths can influence flow characteristics by reducing velocities and the sediment carrying capacities. In such areas, reduced rates of erosion are indicative of areas with large channel widths (Dolan *et al.* 1974). Blinn *et al.* (1992) identified that wide reaches exhibited extremely high total standing crop percentiles in comparison to narrow reaches that were evaluated. We identified that a significant negative correlation exists with channel width to sediment concentration at higher discharges. This indicates that PAR is more available at greater depths in regions having larger channel widths which further supports Blinn's results.

The sediment transport capacity of a discharge dictates the concentration levels, and once sediment particles are actively resuspended, response time is not instantaneous to changes in hydraulic conditions. As documented by Cluer (1992) the sediment transport capacity at 425 m^3/s was approximately 1,300 tons per diem, however, considerably lower then 50% of the experimental test discharges evaluated in the GCES Phase II study.

The suspension of fine sands, silts, and clays from periodic tributary discharges or pre-dam alluvium appears to be cumulative, and once inclined sediment remains in suspension (Laursen and Silverston 1976). This cascading effect maintains sediment in suspension and appears to be related to the fluvial dynamics of each study reach (Graf *et al.* 1989). The sediment transport capacity of the Colorado River and the progressive accumulation of sediment downstream appears to explain the response of increased light attenuation with increasing distances, since the independent geomorphological variables of channel depth, slope and to some extent width appear not to be significant. Also, the lack of an existing correlation to geomorphology may be a factor in attempting to characterize the channel geometry as a mean value representative of a 25 km distance. And yet, using interpolated data that was site specific or at least adjacent to the irradiametric sampling site showed no additional correlation.

Distinct shifts in light attenuation are related to point sources of sediment input from tributaries. The sediment storage differences in the river channel downstream from these confluence areas in addition to other catchment areas may explain these attenuation shifts. As discussed, tributaries will influence the availability of sediment, especially since both the Paria River and LCR contribute 72% of the Colorado River's annual sediment budget (Randel and Pemberton 1987). In addition, differences in water chemistry from the LCR tributary during base flow of 6.5 m^3/s may account for further light attenuation below the LCR (Johnson and Sanderson 1968). The differences in percent change in light attenuation are related to discharge volume, hydraulics, and the availability of alluvial sediment (i.e. bank and channel storage).

As observed, the percent light attenuation at specific sites displayed distinct patterns of attenuation for both discharges. The mirror response at each site suggests that the hydraulic characteristics are unique and site specific. This response pattern in light attenuation is consistent regardless of the different discharges. A dramatic decrease in percent light attenuation occurred at the National Canyon site (20). This accounted for a net change of 50 and 150% decrease from the previous sampling site 15 km upstream for discharges at 142 and 425 m^3/s. It is speculated that in this general area the hydraulic conditions are not conducive for maintaining suspended sediment in the water column.

Light Absorptance and Scattering

Light attenuation equals the sum of the optical properties of scattering and absorptance (Kirk 1983). Due to certain optical conditions loss of irradiance to reflectance may account for a significant portion of the available light for photosynthesis. The quantity of photosynthetically available radiation, *PAR* , is dependent on the presence and physical interaction with particle size, shape, concentration and refractive characteristics which influence the optical properties of the water (Kirk 1980b; Kirk 1983). It is speculated that the primary components of absorptance from

the hypolimnetic releases of Lake Powell's Reservoir are water, dissolved organic and inorganic compounds. In moderate to turbid waters scattering at all angles encompassing the spectrum of visible light (400-700 nm) is primarily due to particles (Kirk 1983). Normal backscattering, b_b , and total scattering coefficients, b , are the most useful types of information for characterizing the scattering properties of water (Kirk, 1980a). Variation in sediment particle size and concentration can significantly affect the optical properties of normal backscattering (Spinrad *et al.* 1978; Kirk 1980a; Kirk 1977). In the Colorado River the optical properties vary both spatially and temporally in response to normal operational discharges, distance downstream from Glen Canyon Dam, and the frequency of sediment contribution from tributaries.

Light attenuation is in part due to the hydraulic characteristics that increase and maintain suspended sediment with increasing distances downstream from Glen Canyon Dam. The progressive increase or abrupt shifts in light attenuation coincide with hydraulically distinct reaches, (refer to Graf *et al.* 1989). In addition, observed differences in light attenuation are attributed to the contrasting differences in sediment storage above and below the Paria and the LCR tributaries. Since 1963, degradational loss of alluvial material has occurred in the Glen Canyon area (Pemberton 1976). Whereas, sediment contribution from the Paria and LCR tributary's has continued to supplement the bed channel loss in sediment (Randel and Pemberton 1987). It is speculated that the sediment storage differences in all reaches below major tributaries account for the additional increases in observed light attenuation.

Our data on absorptance/attenuation (a/K) ratios indicate that the primary constituent responsible for light absorptance in the Glen Canyon area is not sediment. We contend that the shift in ratios of a/K as observed below the Paria tributary are due to sediment differences and availability of sediment both in channel storage and alluvial beaches below major tributaries. Otherwise, the a/K ratios should have remained constant if there was a proportional increase in all attenuating

components. However, *a/K* ratios that shift may account for a nonproportional increase of one of the many components responsible for light attenuation; i.e, soluble dyes, POM and sediment. In addition, sediment data support our contention that the primary component involved in light attenuation below the Paria tributary and progressively downstream is suspended sediment.

The degree of light scattering is dependent on size and concentration of suspended inorganic and organic particulates. Coefficients of normal backscattering have been used to determine suspended sediment concentrations based on the relationship that light attenuation equals the sum of absorptance and normal backscattering, b_b . Studies on the Yellow River in China, using remote sensing methods (Landsat MSS) have identified a correlation between empirical data collected on sediment concentrations with similar estimates using backscattering reflectance (Aranuvachapu and Walling, 1988). In certain situations a linear relationship occurs with suspended matter and the scattering coefficient (Jones and Will 1956). In remote sensing studies, a linear relationship with suspended sediment concentration and scattering is obtained by isolating the red and near infrared waveband. Absorption in the red waveband remains fairly constant, this is principally due to the fact that water is the primary medium of absorptance for this spectral region (Klemas *et al.* 1973; Aranuvachapu and Walling 1988). A linear relationship with suspended sediment will occur only if the absorption coefficient remains constant since reflectance varies inversely with absorptance while increasing with b_b at the 400-700 nm bandwidth (Kirk 1983). However, this method would be impractical for determining sediment concentration due to limitations in river size and background interference from shoreline margin.

Conditions of differing levels of turbidity can influence the spectral distribution of irradiance in addition to the availability of total *PAR* (Kirk 1979). Scattering increases in proportion to concentration with a strong indication that within the visible spectrum of light (400-700 nm) the shorter wavelength becomes easily scattered (Morel 1973). Under minimal tributary flow, non-algal

components either dissolved or colloidal compounds are of an allochtonous source and are generally minimal in concentration; however, their presence can reduce the quality and quantity of PAR for photosynthesis (Kirk 1980a; and Jewson and Taylor 1978). Partial or total elimination of different wavelengths of visible light can influence algal composition and vertical distribution. The adaptive capabilities of different algal species to utilize both the changes in the spectral region and light intensities will influence algal composition and their distribution (Larkum *et al.* 1966). Blinn *et al.* (1992) identifies that algal dominance shifts to favor Oscillatoria downstream from the Little Colorado River. It is speculated that the shift in composition is an adaptive response by this species to tolerate desiccation, light availability and the spectral shift away from the blue waveband.

The optical characteristics of water classified by Kirk (1980a and 1983) indicate that waters with a large particulate fraction will absorb light more strongly than the soluble fraction. Typically, under conditions of high clarity and low soluble dyes, water will have a higher affinity for absorbing the longer waveband (600-700 nm) of the orange-red region. The visible light spectrum shifts in natural waters containing high concentrations of phytoplankton and favors a greater penetration of the red region (Kirk 1979). At this point in time plankton densities in the Colorado River are of such low concentrations that they are considered by us to be an insignificant component of the overall constituents involved in light absorption (Haury, 1986). In conditions of high turbidity the shorter wavelength in the blue (400-500 nm) or blue-green (400-550 nm) region are attenuated in the upper surface (Kirk 1983). This spectral shift eliminates or reduces the utilization of this very important spectral region (400-500 nm). This has negative implications for growth and photosynthetic yield of C. glomerata which utilizes this spectral region (Kirk 1983).

Optical Conditions within the Colorado River's Euphotic Zone

The attenuation of underwater light directly influences the spatial quantity and density of algae

present within the euphotic zone, (Ganf 1974; Jewson and Taylor 1978), gross photosynthetic yields per unit area (Vollenweider 1960), and the temporal rate of growth (Jewson Taylor 1978). Literature supports an adaptation by C. glomerata to low light intensities (Mantai 1974; Lester *et al.* 1974; Adams and Stone 1973). Therefore, a spatial relationship for light attenuation exists as a function not only of depth, but distance and discharge from Glen Canyon Dam.

It can be surmised that periods of exclusion or concealment below the compensation point is another factor controlling vertical zonation of this algae. Resident time of algae below this lower limit restricts growth rate, photosynthetic yield, and areas for colonization (Jewson and Taylor 1978). The time of residence for phytoplankton in non-illuminated zones in turbid lakes has been shown to influence net yields of photosynthesis per unit area and growth (Jewson and Taylor 1978). Increased light attenuation will reduce or totally eliminate certain areas that might otherwise be available for colonization and growth (Spence and Chrystal 1970). This becomes further complicated once you consider the temporal (diel and seasonal) duration and variability of the underwater light regime in the Colorado River. For this reason, it is speculated that colonization and growth are restricted closer to the channel margin during suboptimum light conditions in areas located 150 km downstream or greater from Glen Canyon Dam. In the lower portion of the Grand Canyon this reduction in depth has negative implications for C. glomerata because fluctuating flows may potentially subject the only available area for attachment and growth to the effects of desiccation.

In a different light, a significant factor is exposure time, primarily because of the sessile nature of C. glomerata. Under fluctuating flow regimes, loss in surface area due to channel depth reduction is further compounded by exposure above saturation point potentially resulting in photoinhibition (Mantai 1974; Adams and Stone 1973; Boston and Hill 1991), and desiccation (Usher *et al.* 1987). Studies on exposure of this algae indicated a depreciable effect within the intertidal zone from

desiccation due to fluctuating flow patterns generated by Glen Canyon in the Colorado River (Usher *et al.* 1987). Similar studies have identified effects from desiccation, temperature and light intensities brought about by exposure (Hodgson, 1980; Adams and Stone 1973; and Pantastico and Suayan 1973).

In the Lees Ferry area growth and maintenance of C. glomerata requires a minimum 0.5 m subsurface depth regardless of flow regime (Pinney 1991). Besides the effect of desiccation, this observed depth response may be related to areas exposed at or above the saturation point. Exposure to the red light spectrum has been identified with aging and fragmentation of C. glomerata (Pantastico and Suayan 1975). Mantai (1974) reported that the photosynthetic saturation point occurred at light intensities of 920 μE. Information is not available on intensity levels and duration required to initiate a photoinhibitive response in C. glomerata, however, photoinhibition above the point of light saturation will reduce the photosynthetic rate in all aquatic algae. Research on photoinhibition of phytoplankton, Asterionella, indicates an exponential decline in rate of recovery to the duration of exposure (Kirk 1983; Boston and Hill 1991). Since increased exposure can offset recovery rates subsurface depths with high intensities could limit the upper vertical distribution of C. glomerata in waters having low light attenuation as found in the Glen Canyon area.

Optimum temperatures for photosynthesis of C. glomerata range slightly higher, 13 to 17°C, then the temperatures at Lees Ferry, 8 to 12°C (Pinney 1991). Graham (1982) reported that growth increased in colder temperatures with higher light intensities under controlled laboratory conditions. The inverse was true for warmer temperatures. The maximum net photosynthesis occurs at water temperatures ranging from 13° to 17°C, for light intensities ranging between 300 to 600 μE (Graham *et al.* 1982). During our study the observed temperatures for the entire length of the Colorado River ranged from 8.7 to 17°C (142 m^3/s), and 8.5 to 13.3°C (425 m^3/s). The

contrasting differences observed in temperature were attributed to differences in the surface area and mass of water for each distinct discharge, and its downstream transit time. Due to the colder stenothermic releases from Glen Canyon Dam (Ward and Stanford 1979), the calculated zones for maximum net photosynthesis and the saturation point may slightly overestimate the actual photosynthetic range (Graham *et al.* 1982) for the upper portion of Glen and Grand canyons. And yet, in the middle and lower portions of the Grand Canyon water temperatures are at an optimum for C. glomerata, and may reflect the actual euphotic zone.

Glen Canyon Dam Operations

As identified, discharge volume directly influences the degree of light attenuation and is an independent variable that is directly controlled by operational management decisions. It was identified that variable discharges increases light attenuation in the Lees Ferry area. Certain research flows at varying ramp rates at Glen Canyon Dam were identified as causing greater degradation of alluvial deposits (GCES-Interim Flow Recommendations 1991). If our measurements are an indication of how light attenuation increases above 425 m^3/s in the Glen Canyon reach that is known to be sediment depleted, light attenuation should increase dramatically downstream (Pemberton 1976). The "stair-step" decrease in standing crop of primary producers and macroinvertebrates observed in the Colorado River as associated with the primary tributaries indicates the limiting effect on primary and secondary productivity by sediment (Blinn *et al.* 1992; and Usher *et al.* 1990). Furthermore, it becomes apparent that under a fluctuating flow regime, rapid ascending or descending limbs of the hydrograph would display greater light attenuation than at a constant discharge of similar volume. It is speculated that additional light attenuation would be evident at similar discharges (142 and 425 m^3/s) if ramping rates were factored into this equation (Cluer 1992).

Secondly, operational management of Lake Powell reservoir could further accentuate the observed

light attenuation downstream. The reservoir usually exhibits an extended period of stratification and convective mixing during the winter period, and generally does not extend for the entire reservoir depth (Stanford and Ward 1990; Johnson and Merritt 1979). However, under lower lake levels the withdrawal depth as related to surface elevation of Lake Powell may influence water quality and the attenuating characteristics of that discharge release. Seasonal variation in water clarity of Glen Canyon Dam releases would then result in greater light attenuation. We identified a distinct shift toward greater light attenuation during the winter period. On 16 December 1991, during a period of lake mixing (per comm. Verneiu), irradiametric measurements collected showed an elevated attenuation coefficient of 0.302 (r^2, 0.955) for scalar irradiance (refer to Appendix D). Preliminary data indicates that lower water elevation in the reservoir combined with lake turnover may be responsible for elevated vertical attenuation coefficients. If this water quality condition is prevalent during winter periods the compensation depth would be further reduced, this is also in addition to the reduction in seasonal solar intensities and exposure time expected during this same period. This indicates that the use of a constant K_{avg} for seasonal comparisons is only applicable during conditions conducive for stratification of the reservoir prior to the turnover of the epilimnion.

CONCLUSIONS

Light attenuation is positively correlated to both increasing discharges and distances downstream from Glen Canyon Dam. Suspended sediment is the most significant factor regulating PAR in the Colorado River, Glen and Grand Canyons. The major factors influencing light attenuation are as follows: 1) sediment discharge from major tributaries; 2) discharge releases from Glen Canyon Dam; 3) sediment storage differences below major tributaries; and 4) channel geometry influencing fluvial hydrology. As speculated by Pinney (1991), seasonal changes in light intensity coupled with fluctuating flow levels are the most regulating factors for C. glomerata biomass in Glen Canyon. At present limited information is available on the seasonal shift and duration of exposure of *PAR* and frequency of sediment discharge from tributaries into the Colorado River.

The light absorptance by sediment appears to be a major factor influencing vertical light attenuation. Light scattering by the reflectant properties of sediment increases with downstream distances. Both of these mechanisms in light attenuation have negative implications for the quantity and spectral composition of light available for photosynthesis. Optimum light conditions for photosynthesis are determined by the optical properties of water and exist when the compensation point depth for C. glomerata exceeds the channels mean thalweg depth. It was found that at lower discharges (142 m^3/s) the depth of the river channel does not exceed the lower limits of C. glomerata compensation point for the entire length of Glen and Grand Canyons. These optical conditions are optimal for photosynthesis. However, at higher discharges (425 m^3/s) the depth of the river channel exceeds the lower limits of C. glomerata compensation point. This reduction in vertical depth generates suboptimum light conditions for photosynthesis from the Granite Gorge 150 km to Diamond Creek 387 km. The quantity and availability of light is influenced by the duration of optimum light conditions, frequency between periods of tributary discharges, and the spatial differences in light attenuation downstream from Glen Canyon Dam. The reduction in solar intensities and duration will decrease the total *PAR* available for aquatic productivity.

In addition, the use of other light measuring methods have applications in characterizing *PAR* since correlations have been established with these other methods (e.g. cosine corrected sensors and secchi disc). Vertical attenuation coefficients derived from irradiametric methods using either cosine corrected or scalar sensors are significantly different, but can be made equivalent. Also, secchi depth measurements collected in the Colorado River, Glen and Grand Canyons can be used to derive vertical attenuation coefficients, K_o, for scalar irradiance. Refer to Appendix B for further information regarding techniques for correlating other light measuring techniques.

REFERENCES CITED

Adams, M.S., and W. Stone. 1973. Field studies on photosynthesis of Cladophora glomerata (Clorophyta) in Green Bay, Lake Michigan. Ecology, 54:853-862.

Angradi, T.R. and D.K. Kubly. 1992. Concentration and transport of particulate organic matter below Glen Canyon Dam on the Colorado River, Arizona. Arizona Game and Fish Department, Phoenix, Arizona. Draft Final Report.

Aranuvachapun, S., and D.E. Walling. 1988. Landsat - MSS Radiance as a measure of suspended sediment in the Lower Yellow River (Hwang Ho). Remote Sensing of Environment., 25:145-165.

Boston, H.L. and W.R. Hill. 1991. Photosynthesis-light relations of stream periphyton communities. Limnol. Oceanogr., 36(4):644-656.

Cluer, B.L. 1992. Analysis of sand bar response along the Colorado River in Glen and Grand Canyon Dam, using aerial photography. *In.* Beus, S.S. and C.C. Avrey. 1992. The influence of variable discharge regimes on Colorado River sand bars below Glen Canyon Dam: Draft Final Report.

Colby, B.R. 1961. Effect of depth flow on discharge of bed material. U.S. Geological Survey - Water Supply Paper 1498-D, 12p.

Di Toro, D.M. 1978. Optics of Turbid Esturine Waters: Approximation and Applications. Water Research., 12:1059-1068.

Dolan,R., A. Howard, and A. Gallenson. 1974. Man's Impact on the Colorado River in the Grand Canyon. American Scientist. 62:392-401.

Duchrow, R.M. and W.H. Everhart. 1971. Turbidity measurement. Trans. Amer. Fish Soc., 4:682-690.

Dvihally, S.T. 1961. Seasonal changes in the optical characteristics of a Hungarian sodic lake. Hydrobiologia., 17:193-204.

Einstein, H.A. 1950. The bed-load function for sediment transportation in open channel flows. U.S. Department of Agriculture, Soil Conservation Service, Technical Bulletin 1026 U.S. Government Printing Office, Washington D.C., 71 p.

Gannf, G.G. 1973. Incident irradiance and underwater light penetration as factors controlling the chlorophyll a content of a shallow equatorial lake (Lake George, Uganda). J. Ecol., 62:593-609.

Glen Canyon Environmental Studies - Final Report. 1987. Department of the Interior. National Technical Information Service. PB88-18334.

Glen Canyon Environmental Studies - Interim Flows for Grand Canyon, Recommendation for Interim Operating Procedures for Glen Canyon Dam. 1991. Bureau of Reclamation and the Glen Canyon Studies Cooperating Agencies. April 10, 1991.

Graf, J.B., J.C. Schmidt, and S.W. Kieffer. 1989. Hydraulic log of the Colorado River from Lees Ferry to Diamond Creek, Arizona. *in.* Elston, D.P., G.H. Billingsley, and R.A. Young. Geology of Grand Canyon, Northern Arizona (with Colorado River Guides) Lees Ferry to Pierce Ferry, Arizona. American Geophysical Union, Washington,D.C., 37-48.

Graham, J.M., M.T. Auer, R.P. Canale, and J.P. Hoffman. 1982. Ecological studies and mathematical modeling of Cladophora in Lake Huron: 4. Photosynthesis and respiration as functions of light and temperature., J. Great Lakes Res., 8(1):100-111.

Grande, K.D., J. Marra, C. Langdon, K. Heinemann, and M.L. Bender. 1989. Rates of respiration in the light measured in marine phytoplankton using an ^{18}O isotope-labeling technique. J. Exp. Mar. Biol. Ecol., 129:95-120.

Guy, H.P. 1969. Laboratory theory and methods for sediment analysis. U.S. Geological Survey, Book 5, Chapter CL, U.S. Government Printing Office, Washington,D.C., 1-55.

Hardwick, G.G., D.W. Blinn, and H.D. Usher. 1992. Epiphytic diatoms on Cladophora glommerata in the Colorado River, Arizona: longitudinal and vertical distribution in a regulated river.

Haury, L.R. 1986. Zooplankton of the Colorado River Glen Canyon Dam to Diamond Creek. Glen Canyon Environmental Studies Technical Report. National Technical Information Service. PB88-183462

Herford, R. 1984. Climate and ephemeral-stream processes: Twentieth-century geomorphology and alluvial stratigraphy of the Little Colorado River, Arizona. Geological Society of America Bulletin., No.95, p. 654-668.

Hodgson, L.M. 1981. Photosynthesis of the red alga, Gastrocclonium coutteri (Rhodophyta) in response to changes in temperature, light intensity, and desiccation. J. Phycol., 17:37-42.

Howard, A. and R. Dolan. 1981. Geomorphology of the Colorado River in the Grand Canyon. J. of Geology., 89(3):269-298.

Jewson, D.H. and J.A. Taylor. 1978. The influences of turbidity on net phytoplankton photosynthesis in some Irish lakes. Freshwater Biology., 8:573-584.

Johnson, P.W., and R.B. Sanderson, 1968. Springflow into the Colorado River Lee's Ferry to Lake Mead, Arizona. Water-Resources Report # 34, Arizona State Land Department.

Jones, R.I. and V. Ilmavirta. 1978. A diurnal study of the phytoplankton in the eutrophic lake Lovojarvi, Southern Finland. Arch Hydrobiol., 83(4):491-514.

Jones, D. and M.S. Will, The attenuation of light in sea esturine waters in relation to the concentration of suspended matter. J. Mar. Biol. Ass. U.K., 35:431-444

Kirk, J.T.O. 1977. Use of a quanta meter to measure attenuation and underwater reflectance of photosynthetically active radiation in some inland and coastal South-eastern Australian waters. Aust. J. Mar. Freshwater Res., 28:9-21.

Kirk, J.T.O. 1979. Spectral distribution of photosynthetically active radiation in some South-eastern Australian waters. Aust. J. Mar. Freshwater Res., 30:81-91.

Kirk, J.T.O. 1980a. Relationship between nephelometric turbidity and scattering coefficients in certain Australian waters. Aust. J. Mar. Freshwater Res., 31:1-12.

Kirk, J.T.O. 1980b. Spectral absorption properties of natural waters: Contributions of the soluble and particulate fractions to light absorption in some inland fractions of south-eastern Australia. Aust.J.Mar.Freshwater Res., 31:287-296.

Kirk, J.T.O. 1983. Light and photosynthesis in aquatic ecosystems. Cambridge University Press, Cambridge, London., pg.401

Klemas, V., J.F. Borchardt, and W.M. Treasure. 1973. Suspended sediment observations from ERTS-1. Remote Sensing of Environment., 2:205-221.

Larkum, A.W.D., E.A. Drew, and R.N. Crossett. 1966. The vertical distribution of attached marine algae in Malta. J. Ecology., 55:361-371.

Laursen, E.M. and E. Silverston. 1976. Hydrology and Sedimentation of the Colorado River in Grand Canyon. National Park Service. Final Report Contract No. CX821060030 pg.27.

Lester, W.W., M.S. Adams and E.H. Deltman. 1974. Light and temperature effects on photosynthesis of Cladophora glomerata, (Clorophyta) in Green Bay, Lake Michigan: Model analysis of seasonal productivity. Masters Thesis , Univ. of Wisconsin, Dept of Botany.

Marcus, B.A. 1980. Relationship between light intensity and chlorophyll content in Myriophyllum spicatum L. in Canadice Lake (New York, U.S.A.). Aquatic Botany., 9:169-172.

Mantai, K.E. 1974. Some aspects of photosynthesis in Cladophora glomerata. J. Phycol., 10:288-291.

Pantastico, J.B. and Z.A. Suayan. 1973. Akinete differentiation in Cladophora glomerata Cladophora sp., Part 2.: Interaction among light photoperiod and growth regulators. Kalikasan Phillipp. J. Biol., 2:39-40.

Pemberton, E.L. 1976. Channel changes in the Colorado River below Glen Canyon Dam. In. Proceedings of the Third Federal interagency sedimentation conference, Denver, Colorado. Water Resources Council, Sedimentation Committee. pp. 5, 61-73.

Pemberton, E.L. 1987. Sediment data collection and analysis for five stations on the Colorado River from Lees Ferry to Diamond Creek. Glen Canyon Environmental Studies Technical Report, National Technical Information Service. PB88-183397, p.156

Petzold, T.J. 1972. Volume scattering functions for selected ocean waters. Scripps Institution of Oceanography, San Diego, CA. S10 Ref. 72-78.

Pinney, C.A. 1991. The response of Cladophora glomerata and associated epiphytic diatoms to regulated flow and the diet of Gammarus lacustris, in the tailwaters of Glen Canyon Dam. M.S. Thesis Northern Arizona University. Department of Biology p.82

Randel, T.J. and E.L. Pemberton 1987. Results and analysis of STARS (Sediment Transport and River Simulation) modeling efforts of Colorado River in Grand Canyon. Glen Canyon Environmental Studies Technical Report, National Technical Information Service. PB88-183421, p.190

Roemer, S.C., and K.D. Hoagland. 1979. Seasonal attenuation of quantum irradiance (400-700 nm) in three Nebraska reservoirs. Hydrobiolia., 63:81-92.

Schmidt,J.C., and J.B. Graf. 1988. Aggradation and degradation of alluvial sand deposits 1965 to 1986, Colorado River, Grand Canyon National Park, Arizona. USGS Professional Paper, Open-File Report 87-555. pp.120.

Schmidt,J.C. 1990. Recirculating flow and sedimentation in the Colorado River in Grand Canyon, Arizona. Journal of Geology., 98:709-724.

Scott, B.D. 1978. Phytoplankton distribution and light attenuation in Port Hacking estuary. Aust.J.Mar.Freshwater Res., 29:31-44.

Smith, R.C. 1968. The optical characterization of natural waters by means of an extinction coefficient. Limnol. Oceanogr., 13:423-429.

Spence D.H.N., and J. Chrystal. 1970. Photosynthesis and zonation of freshwater macrophytes. New Phytol., 69:205-215.

Spinrad, R.W., J.R.V. Zaneveld, and H. Pak. 1978. Volume scattering function of suspended particulate matter at near-forward angles: a comparison of experimental and theoretical values. Applied Optics., 17(7):1125-1130.

Stanford, J.A. and J.V. Ward. 1991. Colorado River Ecology and Dam Management Limnology of Lake Powell and the chemistry of the Colorado River. Proceedings of a Symposium May 24-25, 1990. Santa Fe, New Mexico, National Academy Press, Washington D.C. 75-101.

Talling, J.F. 1965. The photosynthetic activity of phytoplankton in East African Lakes. Int. Revueges Hydrobiol. Hydrogr., 50:1-32. *in.* Gannf, G.G. 1973. Incident irradiance and underwater light penetration as factors controlling the chlorophyll A content of a shallow equatorial lake (Lake George, Uganda). J. Ecol., 62:593-609.

Tett, P., C. Gallegos, M.G. Kelly, G.M. Hornberger, and B.J. Cosby. 1978. Relationships among substrate, flow, and benthic microalgal pigment density in the Mechums River, Virginia. Limnol. Oceanogr., 23(4):785-797.

Usher, H.D., D.W. Blinn, G.G. Hardwick, and W.C. Leibfried. 1987. Cladophora glomerata and its diatom epiphytes in the Colorado River through Glen and Grand Canyons: distribution and desiccation tolerance. GCES Report No. B-8., 79pp.

Webb, R.H. 1987. Debris flows from tributaries of the Colorado River, Grand Canyon National Park, Arizona. USGS Professional Paper, Open - File Report 87-117., 120pp.

Williams, D.T., G.R. Drummond, D.E Ford, and D.L. Robey. 1980. Determination of light extinction coefficient in lakes and reservoirs. Surface Water Impoundments., 2:1329-1335.

Wofsy, S.C. 1983. A simple model to predict extinction coefficients and phytoplankton biomass in eutrophic waters. Limnol. Oceanogr., 28(6):1144-1155.

ACKNOWLEDGEMENTS

A special thanks is extended to all the individuals who participated in both the data collection and laboratory analysis; especially, Helen Yard, Jeanie Korn, Michael Schaffer, Valerie Saylor, and Renee Davis. The logistical and technical difficulties encountered on the Colorado River were at times inordinate. The immediate gratification was far from illuminating during the field collection effort and considered by some to be a combined state of monotony and insanity. The patience and hard work of these participants has been greatly appreciated. A special recognition is extended to David Wegner, GCES Program Manager for his support towards this project. In addition, Lawrence Stevens and Dean Blinn were instrumental in their assistance during the developmental process of this study, and their continual advice and direction has improved and shaped this report. Also, the assistance provided by Michael Kearsley and Stephanie Yard in statistical analysis and database organization were at critical junctures in time. This study would have been impossible without the USGS irradiametric and sediment sampling equipment provided by Robert Avret and Robert Hart. Also, Timothy Randel provided useful data from the STAR simulation model on channel bed configuration for our analysis. The technical review of Dean W. Blinn, Steve Heibert, Richard Lechleitner, Lawrence Stevens, and David L. Wegner, have been insightful in developing and structuring this report. Also, the assistance from the Glen Canyon Environmental Studies staff and especially the illustrating and graphic skills of Sherry Jacobs and Renee Davis have been indispensable.

APPENDIX A

TABLES

PHOTOSYNTHETICALLY AVAILABLE RADIATION (PAR)

IN THE COLORADO RIVER: GLEN AND GRAND CANYON

Table 1., Tabulated results from the integrated sediment analysis measured at a constant discharge of 142 cms, collected from 910702 and 910712 to 910715

SAMPLE NO.	DATE	KM	PARTICULATE CONC. g/L	MEAN PARTICULATE CONC. g/L	PARTICULATE SAMPLE CONC. s.d.	MEAN STANDARD ERROR	(POM) ORGANIC CONC. g/L	MEAN ORGANIC CONC. g/L	ORGANIC SAMPLE CONC. s.d.	MEAN STANDARD ERROR	SEDIMENT CONC. g/L	MEAN SEDIMENT CONC. g/L	SEDIMENT SAMPLE CONC. s.d.	MEAN STANDARD ERROR
5K 1A	910628	0.0	0.0099	0.0091	0.0008	0.000482	0.0070	0.0069	0.0003	0.000148	0.0028	0.0022	0.0006	0.000338
5K 1B	910628	0.0	0.0095				0.0071				0.0024			
5K 1C	920628	0.0	0.0079				0.0065				0.0014			
5K 1A-2	910712	0.0	0.0150	0.0126	0.0056	0.003236	0.0130	0.0088	0.0062	0.004417	0.0020	0.0022	0.0016	0.001298
5K 1B-2	910712	0.0	0.0049				*				*			
5K 1C-2	910712	0.0	0.0180				0.0135				0.0045			
5K 2A	910712	24.2	0.0046	0.0063	0.0012	0.000678	*	0.0031	0.0023	0.001593	*	0.0016	0.0012	0.000832
5K 2B	910712	24.2	0.0070				0.0042				0.0028			
5K 2C	910712	24.2	0.0072				0.0052				0.0020			
5K 3A	910712	29.0	0.0126	0.0081	0.0034	0.001990	0.0104	0.0055	0.0043	0.003014	0.0022	0.0013	0.0009	0.000656
5K 3B	910712	29.0	0.0042				*				*			
5K 3C	910712	29.0	0.0076				0.0060				0.0016			
5K 4A	910713	50.8	0.0070	0.0057	0.0011	0.000615	0.0032	0.0023	0.0006	0.000357	0.0038	0.0034	0.0006	0.000328
5K 4B	910713	50.8	0.0058				0.0020				0.0038			
5K 4C	910713	50.8	0.0044				0.0018				0.0026			
5K 5A	910713	77.0	0.0119	0.0099	0.0021	0.001215	0.0083	0.0076	0.0006	0.000359	0.0036	0.0023	0.0015	0.000863
5K 5B	910713	77.0	0.0070				0.0068				0.0002			
5K 5C	910713	77.0	0.0107				0.0077				0.0030			
5K 6A	910713	100.6	0.0064	0.0119	0.0056	0.003234	0.0050	0.0044	0.0034	0.002373	0.0014	0.0014	0.0000	0.000006
5K 6B	910713	100.6	0.0096				0.0081				0.0014			
5K 6C	910713	100.6	0.0196				*				*			
5K 7A	910714	124.0	0.0094	0.0114	0.0023	0.001310	0.0086	0.0094	0.0018	0.001016	0.0008	0.0021	0.0009	0.000526
5K 7B	910714	124.0	0.0103				0.0076				0.0026			
5K 7C	910714	124.0	0.0146				0.0118				0.0028			
5K 8A	910714	126.7	0.0134	0.0132	0.0007	0.000377	0.0094	0.0083	0.0008	0.000470	0.0040	0.0049	0.0007	0.000430
5K 8B	910714	126.7	0.0123				0.0075				0.0048			
5K 8C	910714	126.7	0.0139				0.0080				0.0058			
5K 9A	910715	149.7	0.0032	0.0076	0.0033	0.001917	0.0010	0.0026	0.0013	0.000747	0.0022	0.0050	0.0027	0.001552
5K 9B	910715	149.7	0.0084				0.0042				0.0042			
5K 9C	910715	149.7	0.0113				0.0026				0.0087			
5K 10A	910629	166.6	0.0124	0.0148	0.0024	0.001397	0.0082	0.0093	0.0017	0.000995	0.0042			
5K 10B	910629	166.6	0.0181				0.0117				0.0065			
5K 10C	910629	166.6	0.0139				0.0079				0.0061			
5K 10A-2	910715	166.6	0.0060	0.0096	0.0060	0.003451	0.0030	0.0031	0.0005	0.000288	0.0030	0.0065	0.0055	0.003174
5K 10B-2	910715	166.6	0.0181				0.0038				0.0143			
5K 10C-2	910715	166.6	0.0048				0.0026				0.0022			
5K 13A	910629	201.2	0.0108	0.0083	0.0021	0.001226	0.0038	0.0035	0.0005	0.000272	0.0070	0.0048	0.0017	0.000993
5K 13B	910629	201.2	0.0084				0.0038				0.0046			
5K 13C	910629	201.2	0.0056				0.0028				0.0028			
5K 14A	910630	225.4	0.0225	0.0245	0.0035	0.002034	0.0103	0.0103	0.0015	0.000886	0.0121	0.0142	0.0022	0.001295
5K 14B	910630	225.4	0.0295				0.0121				0.0174			
5K 14C	910630	225.4	0.0216				0.0084				0.0132			
5K 15A	910630	251.1	0.0250	0.0233	0.0022	0.001277	0.0079	0.0066	0.0011	0.000630	0.0171	0.0168	0.0013	0.000775
5K 15B	910630	251.1	0.0202				0.0053				0.0150			
5K 15C	910630	251.1	0.0248				0.0066				0.0182			
5K 18A	910630	275.3	0.0178	0.0180	0.0029	0.001660	0.0064	0.0062	0.0012	0.000715	0.0114	0.0117	0.0017	0.000956
5K 18B	910630	275.3	0.0145				0.0046				0.0099			
5K 18C	910630	275.3	0.0218				0.0077				0.0139			
5K 20A	910701	292.2	0.0253	0.0227	0.0035	0.002001	0.0108	0.0091	0.0026	0.001501	0.0144	0.0136	0.0009	0.000506
5K 20B	910701	292.2	0.0178				0.0054				0.0124			
5K 20C	910701	292.2	0.0251				0.0110				0.0141			
5K 21A	910701	322.7	0.0263	0.0197	0.0047	0.002720	0.0122	0.0084	0.0030	0.001758	0.0141	0.0114	0.0020	0.001170
5K 21B	910701	322.7	0.0172				0.0080				0.0092			
5K 21C	910701	322.7	0.0156				0.0048				0.0108			
5K 22A	910702	350.9	0.0359	0.0375	0.0078	0.004508	0.0119	0.0130	0.0028	0.001603	0.0240	0.0244	0.0051	0.002933
5K 22B	910702	350.9	0.0477				0.0169				0.0309			
5K 22C	910702	350.9	0.0288				0.0103				0.0184			
5K 23A	910702	374.2	0.0040	0.0293	0.0180	0.010377	0.0036	0.0100	0.0052	0.003030	0.0004	0.0193	0.0134	0.007733
5K 23B	910702	374.2	0.0395				0.0098				0.0297			
5K 23C	910702	374.2	0.0444				0.0165				0.0279			
5K 24A	910702	387.9	0.0269	0.0263	0.0050	0.002866	0.0078	0.0092	0.0036	0.002070	0.0191	0.0171	0.0021	0.001184
5K 24B	910702	387.9	0.0199				0.0056				0.0143			
5K 24C	910702	387.9	0.0320				0.0141				0.0180			

Mean Organic (g/L)	0.007497
Organict (s.d.)	0.003625
S.E.	0.000471

Mean Sediment (g/L)	0.008714
Sediment (s.d.)	0.007693
S.E.	0.001001

Data not available (*)

Table 2., Tabulated results from the integrated sediment analysis measured at a constant discharge of 425 m^3/s, collected from 910523 to 910531.

SAMPLE NO.	DATE	KM	PARTICULATE CONC. g/L	MEAN PARTICULATE CONC. g/L	PARTICULATE SAMPLE CONC. s.d.	MEAN STANDARD ERROR	(POM) ORGANIC CONC. g/L	MEAN ORGANIC CONC. g/L	ORGANIC SAMPLE CONC. s.d.	MEAN STANDARD ERROR	SEDIMENT CONC. g/L	MEAN SEDIMENT CONC. g/L	SEDIMENT SAMPLE CONC. s.d.	MEAN STANDARD ERROR
15K1A	910523	0.0	0.0026	0.0038	0.0011	0.000647	*	0.0017	0.0004	0.000299	*	0.0018	0.0013	0.000945
15K1B	910523	0.0	0.0053				0.0021				0.0032			
15K1C	910523	0.0	0.0036				0.0013				0.0023			
15K2A	910523	24.2	0.0051	0.0057	0.0012	0.000668	0.0044	0.0051	0.0016	0.000913	0.0006	0.0006	0.0004	0.000252
15K2B	910523	24.2	0.0073				0.0073				0.0000			
15K2C	910523	24.2	0.0047				0.0038				0.0011			
15K3A	910523	29.0	0.0025	0.0047	0.0036	0.002098	0.0025	0.0042	0.0031	0.001788	0.0000	0.0005	0.0006	0.000322
15K3B	910523	29.0	0.0098				0.0085				0.0013			
15K3C	910523	29.0	0.0017				0.0015				0.0002			
15K4A	910524	50.8	0.0230	0.0139	0.0090	0.006394	0.0126	0.0126	*	*	0.0104	*	*	*
15K4B	910524	50.8	*				*				*			
15K4C	910524	50.8	0.0049				*				*			
15K5A	910524	77.0	0.0066	0.0079	0.0039	0.002730	0.0030	0.0030	0.0000	0.000002	0.0036	0.0049	0.0013	0.000907
15K5B	910524	77.0	*				*				*			
15K5C	910524	77.0	0.0092				0.0030				0.0062			
15K6A	910525	100.6	0.0178	0.0145	0.0049	0.002843	0.0121	0.0078	0.0032	0.001819	0.0057	0.0066	0.0034	0.001976
15K6B	910525	100.6	0.0181				0.0060				0.0112			
15K6C	910525	100.6	0.0075				0.0045				0.0030			
15K7A	910525	124.0	0.0225	0.0223	0.0024	0.001387	0.0066	0.0067	0.0009	0.000521	0.0158	0.0156	0.0015	0.000868
15K7B	910525	124.0	0.0251				0.0078				0.0173			
15K7C	910525	124.0	0.0192				0.0056				0.0137			
15K8A	910525	126.7	0.0231	0.0207	0.0040	0.002332	0.0081	0.0062	0.0016	0.000947	0.0150	0.0145	0.0047	0.002710
15K8B	910525	126.7	0.0240				0.0041				0.0200			
15K8C	910525	126.7	0.0150				0.0065				0.0085			
15K9A	910526	149.7	0.0602	0.0501	0.0189	0.010900	0.0143	0.0117	0.0025	0.001425	0.0460	0.0384	0.0167	0.009615
15K9B	910526	149.7	0.0665				0.0126				0.0539			
15K9C	910526	149.7	0.0237				0.0084				0.0153			
15K10A	910526	166.6	0.0378	0.0386	0.0006	0.000361	0.0165	0.0154	0.0027	0.001559	0.0213	0.0231	0.0026	0.001490
15K10B	910526	166.6	0.0394				0.0181				0.0213			
15K10C	910526	166.6	0.0385				0.0117				0.0268			
15K11A	910526	175.4	0.0380	0.0267	0.0148	0.008536	0.0124	0.0078	0.0037	0.002140	0.0255	0.0190	0.0119	0.006862
15K11B	910526	175.4	0.0058				0.0034				0.0024			
15K11C	910526	175.4	0.0362				0.0070				0.0292			
15K12A	910527	200.0	0.0061	0.0180	0.0213	0.015036	0.0017	0.0046	0.0054	0.003792	0.0044	0.0134	0.0159	0.011244
15K12B	910527	200.0	*				*				*			
15K12C	910527	200.0	0.0478				0.0121				0.0357			
15K13A	910527	201.2	0.0564	0.0477	0.0102	0.005914	0.0097	0.0090	0.0010	0.000554	0.0466	0.0387	0.0093	0.005361
15K13B	910527	201.2	0.0535				0.0096				0.0439			
15K13C	910527	201.2	0.0333				0.0076				0.0257			
15K14A	910527	225.4	0.0455	0.0758	0.0193	0.011152	0.0197	0.0225	0.0028	0.002007	0.0258	0.0267	0.0222	0.015713
15K14B	910527	225.4	0.0798				0.0254				0.0544			
15K14C	910527	225.4	0.1022				*				*			
15K15A	910528	243.8	0.0815	0.0945	0.0098	0.005633	0.0176	0.0151	0.0018	0.001033	0.0638	0.0794	0.0115	0.006634
15K15B	910528	243.8	0.1049				0.0137				0.0912			
15K15C	910528	243.8	0.0972				0.0140				0.0832			
15K16A	910528	251.1	0.0632	0.0629	0.0118	0.006696	0.0105	0.0131	0.0020	0.001137	0.0527	0.0498	0.0111	0.006388
15K16B	910528	251.1	0.0770				0.0153				0.0617			
15K16C	910528	251.1	0.0486				0.0135				0.0351			
15K17A	910528	263.9	0.0852	0.0997	0.0109	0.006268	0.0170	0.0172	0.0005	0.000308	0.0683	0.0824	0.0109	0.006264
15K17B	910528	263.9	0.1024				0.0180				0.0844			
15K17C	910528	263.9	0.1114				0.0168				0.0946			
15K18A	910528	275.3	0.0945	0.0666	0.0247	0.014288	0.0183	0.0127	0.0039	0.002279	0.0762	0.0539	0.0216	0.012490
15K18B	910528	275.3	0.0710				0.0101				0.0609			
15K18C	910528	275.3	0.0343				0.0097				0.0246			
15K19A	910529	278.4	0.0647	0.0586	0.0110	0.006359	*	*	*	*	*	*	*	*
15K19B	910529	278.4	0.0641				*				*			
15K19C	910529	278.4	0.0411				*				*			
15K20A	910529	292.2	0.0665	0.0758	0.0066	0.003814	0.0000	0.0326	0.0163	0.011509	0.0665	0.0380	0.0280	0.019777
15K20B	910529	292.2	0.0800				0.0326				0.0474			
15K20C	910529	292.2	0.0810				*				*			
15K21A	910529	322.7	0.0923	0.0935	0.0009	0.000512	0.0130	0.0221	0.0066	0.003824	0.0793	0.0714	0.0057	0.003315
15K21B	910529	322.7	0.0945				0.0286				0.0659			
15K21C	910529	322.7	0.0937				0.0246				0.0691			
15K22A	910530	350.9	0.0625	0.0836	0.0150	0.008670	0.0122	0.0150	0.0026	0.001472	0.0503	0.0686	0.0132	0.007647
15K22B	910530	350.9	0.0957				0.0145				0.0812			
15K22C	910530	350.9	0.0928				0.0183				0.0745			
15K23A	910530	374.2	0.0792	0.0886	0.0119	0.006851	0.0191	0.0164	0.0019	0.001102	0.0602	0.0722	0.0132	0.007635
15K23B	910530	374.2	0.1053				0.0147				0.0006			
15K23C	910530	374.2	0.0812				0.0154				0.0658			
15K24A	910531	387.9	0.0691	0.0670	0.0016	0.000901	0.0148	0.0132	0.0032	0.001870	0.0542	0.0539	0.0025	0.001426
15K24B	910531	387.9	0.0653				0.0086				0.0567			
15K24C	910531	387.9	0.0667				0.0160				0.0506			

Mean Organics (g/L)	0.0114
Organics (s.d.)	0.0068
S.E.	0.000866

Mean Sediment (g/L)	0.0375
Sediment (s.d.)	0.0290
S.E.	0.003684

Data not available (*)

Table 3 – Irradiametric values calculated at a discharge of 142 m^3/s.

DATE	SITE	KM	K_o	K_d	K_E	a	I(uE)	(M) OBS. Z_{cp}	(M) CAL. Z_{cp}	Tn	Ra	b'_b	b_b	b	Tn/b'_b	Tn/b
910628	1	0.0	0.217	0.227	0.232	0.184	1924	19.17	19.35	NS	NAR	*	*	*	*	*
910712	1	0.0	0.256	0.274	0.272	0.177	1610	15.54	16.39	1.36	NAR	*	*	*	*	*
910712	2	24.2	0.220	0.250	0.255	0.166	2000	19.06	19.06	0.82	NAR	*	*	*	*	*
910712	3	29.0	0.293	0.323	0.323	0.177	1682	13.73	14.33	5.33	NAR	*	*	*	*	*
910713	4	50.8	0.359	0.380	0.384	0.202	1646	11.17	11.71	2.51	0.0737	0.056	0.018	0.95	44.84	2.63
910713	5	77.0	0.343	0.368	0.373	1.970	1928	12.13	12.23	1.94	NAR	*	*	*	*	*
910714	6	100.6	0.348	0.400	0.421	0.205	1499	11.25	12.08	1.70	NAR	*	*	*	*	*
910714	7	124.0	0.280	0.318	0.324	0.208	2199	15.33	14.99	1.40	NAR	*	*	*	*	*
910715	8	126.7	0.349	0.379	0.389	0.233	1828	11.79	12.05	2.02	NAR	*	*	*	*	*
910715	9	149.7	0.351	0.339	0.341	0.213	1817	11.68	11.96	1.87	0.0732	0.050	0.016	0.85	37.74	2.21
910629	10	166.6	0.458	0.468	0.467	0.271	1808	8.95	9.17	3.12	0.0890	0.083	0.025	1.35	37.43	2.31
910629	13	201.2	0.538	0.554	0.550	0.275	1599	7.39	7.80	4.00	0.1088	0.121	0.035	1.84	33.17	2.18
910630	14	225.4	0.527	0.542	0.543	0.293	1362	7.25	7.98	3.32	0.1135	0.123	0.035	1.85	27.01	1.8
910630	16	251.1	0.576	0.644	0.665	0.376	2044	7.34	7.30	3.32	0.1135	0.146	0.041	2.19	22.73	1.51
910630	18	275.3	0.612	0.613	0.608	0.294	1742	6.64	6.87	4.24	0.1228	0.151	0.042	2.20	28.18	1.936
910701	20	292.2	0.493	0.531	0.538	0.278	1687	8.18	8.52	3.47	0.1228	0.130	0.036	1.91	26.57	1.82
910701	21	322.7	0.645	0.600	0.598	0.305	1801	6.35	6.51	3.71	CBR	*	*	*	*	*
910702	22	350.9	0.569	0.561	0.561	0.275	1407	6.77	7.39	3.68	0.1039	0.117	0.034	1.80	31.55	2.04
910702	23	374.2	0.662	0.678	0.688	0.357	2030	6.37	6.35	4.10	CBR	*	*	*	*	*
910702	24	387.9	0.665	0.690	0.697	0.343	1637	6.01	6.31	4.62	0.0999	0.138	0.041	2.16	33.53	2.14

* NS = No Sample; NAR = No Asymptotic Reflectance; and CBR = Channel Bed Reflectance

Table 4 – Irradiametric values calculated at a discharge of 425 m^3/s.

DATE	SITE	KM	K_o	K_d	K_E	a	I(uE)	(M) OBSER Z_{cp}	(M) CALCULATED Z_{cp}	Tn	Ra	b'_b	b_b	b	Tn/b'_b	Tn/b
910523	1	0.0	0.239	0.230	NS	*	1919	17.39	17.56	1.30	CBR	*	*	*	*	*
910523	2	24.2	0.242	0.247	NS	*	1931	17.23	17.37	2.83	CBR	*	*	*	*	*
910523	3	29.0	0.283	NS	NS	*	1466	13.73	14.83	0.90	CBR	*	*	*	*	*
910524	4	50.8	0.299	0.315	NS	*	1839	13.77	14.05	0.87	CBR	*	*	*	*	*
910524	5	77.0	0.389	0.398	NS	*	489	7.18	10.80	0.57	CBR	*	*	*	*	*
910525	6	100.6	0.351	0.368	NS	*	1679	11.47	11.97	1.23	CBR	*	*	*	*	*
910525	7	124.0	0.392	NS	NS	*	2132	10.87	10.71	5.13	*	*	*	*	*	*
910525	8	126.7	0.465	0.506	NS	*	1861	8.87	9.02	4.60	CBR	*	*	*	*	*
910526	9	149.7	0.689	0.769	NS	*	1866	5.99	6.10	5.83	CBR	*	*	*	*	*
910526	10	166.6	0.706	0.743	NS	*	1534	5.57	5.95	5.87	CBR	*	*	*	*	*
910527	13	201.2	1.077	1.074	NS	*	1525	3.65	3.90	5.77	0.0927	0.199	0.060	3.19	28.96	1.81
910527	14	225.4	0.893	1.050	NS	*	1532	4.40	4.70	6.20	CBR	*	*	*	*	*
910528	16	251.1	1.085	1.002	NS	*	1743	3.74	3.87	6.03	0.0999	0.200	0.059	3.13	30.13	1.93
910528	18	275.3	1.093	1.128	NS	*	1658	3.67	3.84	6.73	0.0999	0.225	0.067	3.53	29.87	1.91
910529	20	292.2	0.735	0.753	NS	*	1782	5.56	5.71	5.43	CBR	*	*	*	*	*
910529	21	322.7	1.169	1.131	NS	*	1536	3.37	3.59	7.90	1.0520	0.238	0.069	3.66	33.20	2.16
910530	22	350.9	0.923	0.933	NS	*	1766	4.41	4.55	5.63	CBR	*	*	*	*	*
910530	23	374.2	0.927	1.047	NS	*	1839	4.44	4.53	5.87	0.1057	0.221	0.064	3.40	26.51	1.73
910531	24	387.9	1.033	1.079	NS	*	231	1.98	4.07	8.20	CBR	*	*	*	*	*

* NS = No Sample; NAR = No Asymptotic Reflectance; and CBR = Channel Bed Reflectance

Table 5, Discharge 142 cms, geomorphological characteristics for channel topography are calculated from STARS Simulation Model data, correlated to irradiametric reach designation. These data are derived from bed material maps supplied by USGS.

SITE	LOCATION KM	MEAN THALWEG DEPTH (M)	MEAN STANDARD ERROR (M)	TOP WIDTH (M)	MEAN STANDARD ERROR (M)	SLOPE	Ko	Zcp (M)
1	0.0	*	*	*	*	*	0.217	19.4
2	24.2	*	*	*	*	0.00124	0.220	19.1
3	29.0	5.99	0.87	284.69	19.58	0.00124	0.293	14.3
4	50.8	6.43	0.64	159.05	6.18	0.00144	0.359	11.7
5	77.0	6.28	0.75	185.09	6.44	0.00153	0.343	12.2
6	100.6	5.31	0.68	260.41	9.23	0.00078	0.348	12.1
7	124.0	5.55	0.87	269.06	17.23	0.00123	0.280	15.0
8	126.7	3.45	0.67	293.55	19.67	0.00198	0.349	12.0
9	149.7	4.64	0.52	204.01	14.54	0.00258	0.351	12.0
10	166.6	5.69	0.57	185.51	8.94	0.00190	0.458	9.2
13	201.2	5.75	0.58	142.17	5.97	0.00215	0.538	7.8
14	225.4	7.07	0.65	153.26	6.46	0.00156	0.527	8.0
16	251.1	5.68	0.69	158.24	6.90	0.00187	0.576	7.3
18	275.3	5.21	0.51	134.70	6.27	0.00112	0.612	6.9
20	292.2	4.11	0.33	165.80	9.70	0.00081	0.493	8.5
21	322.7	3.49	0.25	174.10	9.69	0.00137	0.645	6.5
22	350.9	4.07	0.43	236.54	11.66	0.00128	0.569	7.4
23	374.2	5.41	0.67	188.77	16.39	0.00127	0.662	6.3
24	387.9	5.81	1.40	225.85	21.31	0.00124	0.665	6.3

* Missing values as indicated { * } are not avialable.

Mean geomorphic values for each irradiametric site are based on 1/2 the distance both upstream and downstream from the adjacent irradiametric sites of equal distances.

Table 6 – Discharge 425 cms, geomorphological characteristics for channel topography are calculated from STARS Simulation Model data, correlated to irradiametric reach designation. These data are derived from bed material maps supplied by USGS.

SITE	LOCATION - KM	MEAN THALWEG DEPTH (M)	MEAN STANDARD ERROR (M)	TOP WIDTH (M)	MEAN STANDARD ERROR (M)	SLOPE	Ko	Zcp (M)
1	0.0	*	*	*	*	*	0.239	17.6
2	24.2	*	*	*	*	*	0.242	17.4
3	29.0	7.65	0.88	302.33	18.67	0.00113	0.283	14.8
4	50.8	8.34	0.66	174.42	6.60	0.00144	0.299	14.0
5	77.0	7.93	0.77	200.16	6.45	0.00154	0.389	10.8
6	100.6	6.68	0.71	278.40	10.44	0.00082	0.351	12.0
7	124.0	5.77	0.88	304.23	17.85	0.00126	0.392	10.7
8	126.7	4.93	0.70	296.19	20.28	0.00198	0.465	9.0
9	149.7	6.18	0.57	227.93	15.51	0.00255	0.689	6.1
10	166.6	7.20	0.59	201.99	8.75	0.00190	0.706	5.9
13	201.2	7.76	0.60	162.26	5.61	0.00216	1.077	3.9
14	225.4	8.68	0.68	175.87	6.45	0.00164	0.893	4.7
16	251.1	7.63	0.72	179.51	6.82	0.00182	1.085	3.9
18	275.3	7.17	0.55	153.29	5.76	0.00117	1.093	3.8
20	292.2	6.26	0.34	195.25	9.48	0.00080	0.735	5.7
21	322.7	5.27	0.28	205.07	10.30	0.00141	1.169	3.6
22	350.9	5.84	0.48	258.77	11.38	0.00128	0.923	4.6
23	374.2	7.24	0.72	205.62	15.61	0.00141	0.927	4.5
24	387.9	6.98	1.43	236.50	20.69	0.00203	1.033	4.1

* Missing values are indicated as { * }.

Mean geomorphic characteristics for each irradiametric site are based on 1/2 the distance both upstream and downstream from the adjacent irradiametric sites.

APPENDIX B

METHODS FOR DETERMINING PAR

(ATTENUATION, ABSORBANCE, SCATTERING, AND COMPENSATION DEPTHS)

AND

CORRELATION TECHNIQUES FOR OTHER METHODS OF LIGHT MEASUREMENT

METHODS FOR DETERMINING PAR:

Vertical Light Attenuation, (K)

One way to characterize optical properties of water is to determine the coefficient of extinction or attenuation (Wofsy 1983; Kirk 1977; Roemer and Hoagland 1979). The attenuation of *PAR* is described by the declining slope of subsurface irradiance, referred to as the attenuation coefficient, K . The attenuation coefficient can be calculated using a natural log regression of *PAR* measured at a series of depth intervals. This coefficient is considered one of the best descriptors for assessing the photosynthetic characteristics and capacities of water (Smith 1968; Kirk 1977; Kirk 1983).

Subsurface intensities for all depths have been transformed to natural log values. The results of the linearization of subsurface intensities are exemplified in Fig. 11, illustrating progressive light attenuation for scalar irradiance at different sites located downstream from Glen Canyon Dam. Elevated attenuation coefficient values for K represent greater light attenuation. The differences in attenuation slope, K_o , between Site 2 (23.8 km), Site 9 (149.4 km) and Site 18 (276.3 km) demonstrates how light penetration is appreciably reduced downstream from Glen Canyon Dam.

Light Absorptance, (a)

As identified by Kirk (1977), a better understanding of the factors that contribute to light attenuation would be known if additional types of measurements were collected in conjunction with standard irradiametric measurements of total *PAR*. The absorptance coefficient, a , for a 400-700 nm bandwidth was determined *in situ* by a combination of measurements collected for downward, E_d , and upward irradiance, E_u , using cosine corrected sensors, and scalar irradiance, E_o using omni-directional sensors. This coefficient, a , represents the sum of the absorptive components consisting of water, soluble dyes, sediment, and organic particulates.

Figure 11 – Vertical attenuationcoefficients, (K_d), for cosine corrected measured at two steady state discharges of 142 m^3/s and 425 m^3/s on the Colorado River from Glen Canyon Dam (0 km) to Diamond Creek (387 km).

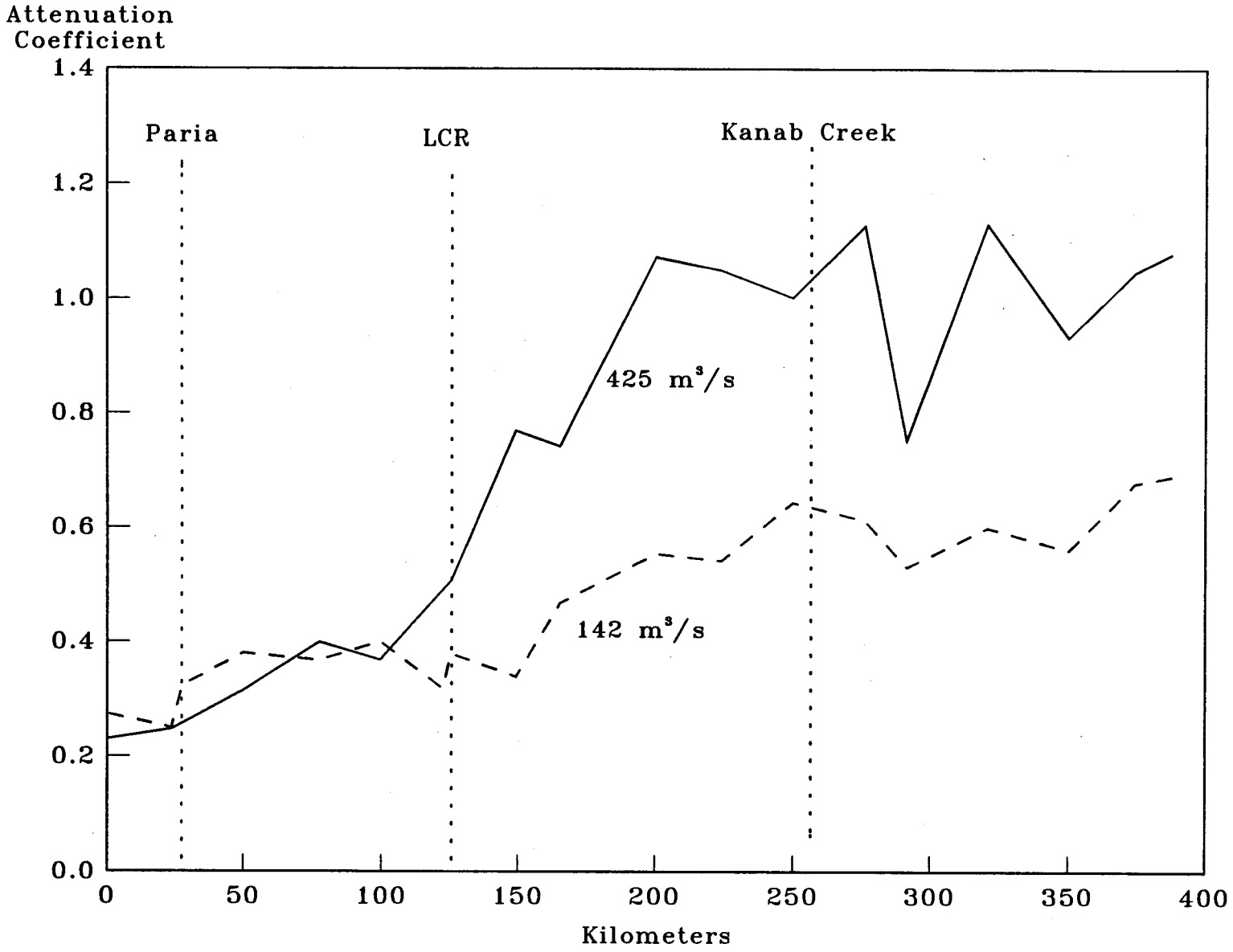

As suggested by Kirk (1983), the method for determining absorption coefficients *a* used in this study are based on the relationship expressed by eqn. 11.

$$a = K_E E/E_o \qquad (11)$$

The absorption coefficient was determined using values for scalar irradiance, E_o , and net downward irradiance, E , consisting of the difference between downward irradiance, E_d , and upward reflectance, E_u , collected at a specific depth. The vertical attenuation coefficient, K_E , is derived from a natural log regression of net downward irradiance, E , for the entire depth profile.

Site differences for absorption coefficients were compared using a constant optical depth of 2.3 which represented the euphotic zones midpoint, Z_m . The value 2.3 is the semi-log value of 10% of *PAR*. The absorption coefficient for a given depth differs slightly due to water surface variability and channel reflectance. The selection of Z_m compensated for the variability in absorbance observed throughout the depth profile. The calculated absorption coefficient, a , at Z_m , and the measured absorptance range for the entire depth profile are depicted in Fig 7. The *in situ* measurement represents the total absorption spectra including the absorptive constituents of water, dissolved and particulate color, and particulates of inorganic and organic nature.

Light Scattering, (b)

Total scattering and normal backscattering coefficients are very difficult to measure either *in situ* or laboratory settings. An alternative approach has been suggested by Kirk (1980a) for calculating different scattering coefficients. Irradiametric data were used to determine the asymptotic backscattering coefficient, b'_b . A relationship exists for asymptotic reflectance and scattering, founded on the theory that any horizontal or vertical reflectance in water is a result of a backscattering (90-180°) phenomena (Kirk 1977, Kirk 1980a). Asymptotic backscattering

coefficient, b'_b , defined as the portion of downward irradiance scattered backwards (180°) is easily measured in the field using the collected irradiametric data at the depth where the ratio of upward reflectance, E_u , to downward irradiance, E_d , quanta irradiance reaches a point of equilibrium.

The asymptotic reflectance, R_a , is determined by assuming that the attenuation coefficient, K , does not change with depth (Kirk 1983). The depth at which asymptotic reflectance, R_a , occurs in the Colorado River was considered the leveling off point of the reflectance ratio, E_u / E_d (Di Toro 1978; Kirk 1977; and Kirk 1980). A multiple line regression was used to determine the line intercept. It was possible to calculate the asymptotic backscattering coefficient, b'_b , by using eqn. 12 (Kirk 1980a).

$$b'_b = 2 \cdot R_a \cdot K \qquad (12)$$

Though important, the conversion of the measured asymptotic backscattering coefficient, b'_b , to a more useable form such as normal backscattering coefficient, b_b , or total scattering coefficient, b, provides more insightful information on the actual scattering properties of water. Normal backscattering, b_b , is determined using the data assembled by Kirk (1980a) for irradiant distributional data of varying turbidities. A linear relationship has been established for known values of asymptotic reflectance, R_a , to ratios of asymptotic backscattering coefficient and normal backscattering coefficients, b'_b / b_b , for varying levels of turbidity. The regression equation (eqn. 13) used for determining the normal backscattering coefficient was developed from tabular data compiled by Kirk (1980a) to determine normal backscattering coefficients.

$$b'_b / b_b = 10.468 \cdot R_a + 2.342, \; R^2 = 0.984 \qquad (13)$$

Normal backscattering coefficient, b_b , are derived by dividing the conversion ratio b'_b / b_b into the calculated value for asymptotic backscattering, b'_b . Total scattering coefficient, b , can be determined using the mean value for the normal backscattering coefficient of 0.0190 m^{-1} (Petzold 1972) relative to the total scattering coefficient of 1.0 m^{-1} (Kirk 1980). The total scattering coefficient, b , equals the value of b_b multiplied by 53, a factor derived from the ratio of b_b to b. This relationship was developed through Petzold's research (1972) on scattering functions for oceanic waters. Additional information specific to the methods for deriving different types of scattering coefficients, b'_b , b_b , and b and their relationships are treated in great detail by both Kirk's (1977; 1980a; and 1983) and Petzold's (1972) research.

Compensation Depth, Z_{cp} :

The euphotic zone depth, Z_{eu} , defined as 1% of *PAR*, has been used by researchers for estimating the extent of the underwater light regime. Talling (1965), identified a relationship between the optical depth of 3.7 and the measured attenuation coefficient K for East African lakes where light attenuation was attributed to high densities of phytoplankton (Ganf 1974). The use of this value and the inverse relationship between euphotic zone, Z_{eu} , and the vertical attenuation coefficient, K , have been verified in other lakes of similar optical conditions. Kirk (1983) identified the use of 4.6 as a constant representing the natural log relationship of 1% PAR. This logrythmic relationship provides a sufficient estimator of the euphotic zone depth for waters similar to those of the Colorado River, expressed as $Z_{eu} = 4.6/K$. However, this relationship does not take into account vertical movement of the euphotic zone due to incidental light variation encountered during seasonal and diel shift of the photoperiod or atmospheric conditions. The optical depth relationship of $4.6/K$ was not considered as reliable a method for determining actual or calculated compensation points because of the possibility of either overestimating or underestimating the actual depth.

As an alternative method we suggest using an equation for calculating depths for the compensation

point Z_{cp}. The natural log value for surface intensity, I , subsurface intensity, I_{ss} , and the attenuation coefficient, K , are used for determining actual depths and calculated depths at variable surface intensities. These depths were calculated by solving for the line-intercept using the attenuation slope (K) and the mean incidental light intensity measured during the depth profile. The compensation point depth equation used is expressed in eqn. 14.

$$Z_{cp} = -1/K \cdot \ln I + 1/K \cdot \ln I_{ss}. \quad (14)$$

The natural log values for surface intensity, I , subsurface intensity, I_{ss} , and the attenuation coefficient, K , are used for determining actual depths and calculated depths in the equation. The value 3.4 is a natural log transformation of 30 μE which represents the compensation point for C. glomerata (Graham 1982). This constant (3.4) specific to C. glomerata or other aquatic algae sharing similar compensation points and is expressed in eqn. 15, having been derived from the above equation.

$$Z_{cp} = 3.4 - \ln I / K \quad (15)$$

The calculated compensation depths, Z_{cp}, at a constant 2000 μE surface intensity allow for a depth comparison between sites and discharges by controlling the incidental light source. We were unable to collect a representative sample of subsurface intensities at all sites; therefore, subsurface intensities were not used because consistency in data collection were often hampered by a wide range of incidental solar flux or quanta sensor movement within the air-water interface. Due to problems encountered in measuring subsurface intensities, I_{ss} , in a riverine environment, we elected to replace actual subsurface values with incidental light intensities, I. For comparative reasons, incidental surface intensities were adjusted to 2000 μE and used with the attenuation coefficient, K , for calculating the compensation depth rather then the actual *in situ* compensation depth.

It was found that the calculated compensation depth underestimates the compensation depth for scalar irradiance using surface values rather than subsurface values. However, measurements based on incidental surface readings are more consistent and allow for comparisons between sites. The mean difference in calculated depth are 0.28 m ± 0.16 (s.d.), based on subsurface measurements to incidental light measurements.

CORRELATIONS BETWEEN SCALAR IRRADIANCE AND LIGHT MEASUREMENT METHODS

Correlations for Downward Irradiance

Vertical attenuation coefficients for scalar irradiance, K_o , and downward (cosine corrected) irradiance, K_d , of *PAR* were calculated for each sample site and replicated at each of the different research flows (142 and 425 m^3/s). Attenuation coefficients for scalar irradiance, K_o , and cosine corrected irradiance, K_d , are graphically depicted (Fig 12 and 13) and the tabulated results for each site are in Tables 3 and 4. Data analysis specific to each site and discharge are found in Appendix D.

Vertical attenuation coefficients derived from measurements of scalar irradiance and downward irradiance are significantly different (paired-t = -3.346, df = 1,36 , p = 0.00193). In the Colorado River under identical optical light conditions total *PAR* will be slightly underestimated using attenuation coefficients derived from downward irradiance, K_d . However, using a regression equation downward irradiance, K_d , can be made equivalent ($F_{1,35} = 1719.3$; $p < 0.0001$) to scalar irradiance, K_o . This equation (eqn. 16) will allow researchers to interrelate data collected using different sensor types for measuring quanta irradiance.

$$K_o \equiv 0.978 \cdot K_d - 0.00957 \quad (R^2_{adj} = 0.979) \qquad (16)$$

Correlations for Secchi Depth

Secchi depth measurements are a standard limnological tool for measuring depths of light reflectance. A method has been developed from our analysis to determine vertical attenuation coefficients from secchi depths collected in the Colorado River. Based on the degree of water clarity two separate regressions were developed for correlating secchi depth measurements, Z_{SD}, to attenuation coefficients, K_o, for scalar irradiance. The selection of the proper equation is dependent on the maximum secchi depth measurement; for depths measured $\geq$ 2.7 m select eqn. 17;

$$K_o = -0.243 \cdot \ln Z_{SD} + 0.711, \ (R^2 = 0.892) \qquad (17)$$

and for depths $\leq$ 2.7 m, select eqn. 18,

$$K_o = -0.857 \cdot \ln Z_{SD} + 1.243, \ (R^2 = 0.868) \qquad (18)$$

A relationship of secchi depths in excess of 8 m to light attenuation has not been effectively developed at this point in time.

APPENDIX C

MANAGEMENT CONSIDERATIONS FOR EIS-ALTERNATIVES:

MANAGEMENT CONSIDERATIONS FOR EIS-ALTERNATIVES:

The proposed alternatives for the operations at Glen Canyon Dam are sure to affect the availability of light for photosynthesis in the Colorado River. The optical properties of water are functionally controlled by the attenuating components which include water, soluble dyes, and suspended organic and particulate organic material. At present the primary light attenuating component in the Colorado River is suspended sediment. The complex interaction between the hydrology, geomorphology, and sediment contribution influence the processes of sediment storage, transport, degradation and aggradation in the riverine system. In regards to the operations of Glen Canyon Dam, certain EIS-alternatives pose both negative and positive affects to light availability and the potential photosynthetic productivity. An understanding of the factors which control primary production during periods of optimum and semi-optimum light conditions need to be further investigated. Discussed below, is a review of each EIS-alternative as it applies to photosynthetically available light.

Year Round Steady Flow

Low steady flows (142 m^3/s) have been observed to decrease sediment transport capacity which would result in lower light attenuation (Cluer 1992), (refer to Table 1, and Fig. 3). These types of flows would potentially reduce transport of suspended sediment and increase available light except for periods of sediment discharge from tributaries above base flow. However, as identified in Fig. 9, a reduction in submerged area available for photosynthesis occurs due to changes in the vertical stage discharge. Discharge volume adjusts to the channel topography as mean channel depth and top width shift in response to changes in vertical stage (Randel and Pemberton 1987).

High steady flows (425 m^3/s) appear to increase the transport and suspension of alluvial sediment stored in the river channel and banks and thereby increasing light attenuation, (refer to Table 2, and Fig. 4). Secondly, a cascading affect results in sediment remaining in suspension into downstream

areas hydrologically similar to areas upstream having low light attenuation (Fig. 1.5). It is speculated that during periods of steady flood flows comparable to 1983-86, would further amplify the light attenuating process in the river. As identified by Pemberton (1987), measurements for suspended sediment concentrations increased during these flood periods. High steady flows would create semi-optimum light conditions for photosynthesis by reducing the compensation point for C. glomerata above a 4 m depth. Partial light extinction would further reduce available area for colonization and algal growth. The affect on production would be more restrictive from the Granite Gorge (150 km) to Diamond Creek (387 km), (refer to Fig. 10).

Seasonally Adjusted Steady Flows

Seasonally adjusted steady flows have the potential to optimize light availability by seasonally adjusting discharge volume with regard to sediment discharge from the primary tributaries (e.g. Paria, LCR, and Kanab Creek). However, higher flows during high delivery months (April - June) would increase light attenuation through the transport and storage of alluvial sediment in the river channel than during low steady flows that occur during months of high tributary runoff (Herford 1984; and Graf *et al.* 1991).

Existing Monthly Volume Steady Flows

As with seasonally adjusted steady flows light availability would increase during low steady flows but would be decreased during higher water delivery months. These critical delivery periods generally coincide during the same time periods when there are minimal input of sediment from tributaries. At these time periods there is a high percentage of available days for optimum light conditions. The effect from this flow alternative is hard to predict since little is known about either the fluvial dynamics or resident time of sediment storage in the channel bed under various flow scenarios. Until such an understanding exists, it will be difficult predicting the sediment available for transport and the corresponding attenuation of light in the water column.

Low Fluctuating Flows

As discussed above, Low Fluctuating Flows would probably result in higher light attenuation than a comparable discharge volume under steady flow conditions. However, the degree of light attenuation increase is unknown and is dependent on the stability of alluvial and channel deposits.

Moderate Fluctuating Flows

Moderate Fluctuating Flows would probably further increase light attenuation than low fluctuating flows. The response time and residency of sediment in suspension with the declining limb of the hydrograph are unknown. As identified in Fig. 4, the reduction in suspended sediment concentration is not instantaneous in geographical reaches where there are distinct hydrological changes.

High Fluctuating Flows

High fluctuating flows are expected to have the same effect on the availability of light as the No Action Alternative.

No Action Alternative

During periods of tributary base flow, the availability of light in irradiametric reaches below the confluence of the Little Colorado River will remain for large periods of time under sub-optimum to light extinction conditions. Secondly, the diel pattern of discharge releases will become synchronized with the photoperiod sustaining certain portions of the river corridor under a particular discharge regimen, (i.e., high-descending and low ascending). The exception to this would be the weekly disruption in discharge volume as week-day releases shift into week-end releases.

ADDITIONAL ELEMENTS TO FLOW ALTERNATIVES

Beach Protection

This would probably have a positive affect on the amount of light available for photosynthesis by stabilizing alluvial sediments that would otherwise be re-suspended during degradational flow patterns.

Beach/Habitat Building Flows

These flows would have negative impacts to availability of light during the actual flow event. The quasi-equilibration rate of alluvial deposition after these flows are unknown. If these flows are implemented they should be timed to coincide with sediment discharge from downstream tributaries to avoid either additional light attenuation or extinction which normally results during these events.

Sediment Augmentation

Sediment augmentation would have a negative impact on the availability of light for photosynthesis. If sediment augmentation is implemented it should be timed to coincide with high sediment discharge from tributaries which would otherwise cause light extinction. It is speculated, that large inputs of sediment into the river system would readjust the sediment storage in the river channel; this additional sediment would be potentially available for transport. This would probably result in increasing light attenuation. Differences in light attenuation and storage of alluvial sediment were observed when comparing dissimilarities above and below both the Paria and the Little Colorado River tributaries.

Multi-level Withdrawal Intake Structure

The optical properties found in the river are affected by the light attenuating constituents in the water source. Increases in turbidity from suspended inorganic and organic material would further

attenuate the optical properties of the river. These attenuating changes have been observed, but the degree of maximum light attenuation are difficult to assess.

APPENDIX D

REGRESSION ANALYSIS FOR STUDY SITES

MEASURED AT DISCHARGES OF 142 AND 425 m^3/s

Site 1, Date 910523, Time: (1053–1119)
Discharge 425 m^3/s
Location: 0.0 km

Regression Output:		Terrestrial Intensity	
Constant	7.447537	Minimum	1851
Std Err of Y Est	0.315995	Maximum	1978
R Squared	0.741284	Mean	1919.2
No. of Observations	50	Std.	34.857
Degrees of Freedom	48		

Ko Coefficient(s)	0.239180
Std Err of Coef.	0.020395

Site 1, Date 910628, Time: (1339–1419)
Discharge 142 m^3/s
Location: 0.0 km

Regression Output:		Terrestrial Intensity	
Constant	7.469774	Minimum	1853
Std Err of Y Est	0.106654	Maximum	2003
R Squared	0.981853	Mean	1923.571
No. of Observations	63	Std.	45.21
Degrees of Freedom	61		

Ko Coefficient(s)	0.217134
Std Err of Coef.	0.003779

Site 1, Date 911216, Time: (1239–1317)
Discharge 376–396 m^3/s
Location: 0.0 km

Regression Output:		Terrestrial Intensity	
Constant	5.774843	Minimum	245.1
Std Err of Y Est	0.144084	Maximum	386.6
R Squared	0.955023	Mean	289.4864
No. of Observations	303	Std.	32.388
Degrees of Freedom	301		

Ko Coefficient(s)	0.302935
Std Err of Coef.	0.003789

Site 1, Date 910712, Time: (0933–1008)
Discharge 142 m^3/s
Location: 0.0 km

Regression Output:		Terrestrial Intensity	
Constant	7.444679	Minimum	1521
Std Err of Y Est	0.073927	Maximum	1672
R Squared	0.995151	Mean	1609.557
No. of Observations	61	Std.	44.992
Degrees of Freedom	59		

Ko Coefficient(s)	0.256243
Std Err of Coef.	0.002328

Site 2, Date 910523, Time: (1348–1421)
Discharge 425 m^3/s
Location: 23.8 km

Regression Output:		Terrestrial Intensity	
Constant	7.566477	Minimum	1854
Std Err of Y Est	0.044145	Maximum	2004
R Squared	0.996225	Mean	1930.756
No. of Observations	41	Std	25.814
Degrees of Freedom	39		

Ko Coefficient(s)	0.241757
Std Err of Coef.	0.002382

Site 2, Date 910712, Time: (1127–1213)
Discharge 142 m^3/s
Location: 23.8 km

Regression Output:		Terrestrial Intensity	
Constant	7.579088	Minimum	1946
Std Err of Y Est	0.041991	Maximum	2032
R Squared	0.995933	Mean	1999.548
No. of Observations	62	Std.	19.797
Degrees of Freedom	60		

Ko Coefficient(s)	0.220369
Std Err of Coef.	0.001817

Site 2, Date 910711, Time: (1334–1413)
Discharge 759–770 m^3/s
Location: 23.8 km

Regression Output:	
Constant	7.666379
Std Err of Y Est	0.052339
R Squared	0.990049
No. of Observations	46
Degrees of Freedom	44

Terrestrial Intensity	
Minimum	1906
Maximum	2006
Mean	1946.675
Std.	30.225

Ko Coefficient(s)	0.30203
Std Err of Coef.	0.004564

Site 3, Date 910523, Time: (1528–1556)
Discharge 425 m^3/s
Location: 27.74 km

Regression Output:	
Constant	7.340761
Std Err of Y Est	0.123147
R Squared	0.972477
No. of Observations	44
Degrees of Freedom	42

Terrestrial Intensity	
Minimum	1410
Maximum	1560
Mean	1466.113
Std.	39.842

Ko Coefficient(s)	0.28326
Std Err of Coef.	0.007353

Site 3, Date 910712, Time: (1433–1524)
Discharge 142 m^3/s
Location: 27.74 km

Regression Output:	
Constant	7.537181
Std Err of Y Est	0.065858
R Squared	0.987876
No. of Observations	54
Degrees of Freedom	52

Terrestrial Intensity	
Minimum	1624
Maximum	1773
Mean	1681.9
Std.	44.212

Ko Coefficient(s)	0.293177
Std Err of Coef.	0.004503

Site 4, Date 910524, Time: (1016–1052)
Discharge 425 m^3/s
Location: 50 km

Regression Output:	
Constant	7.572673
Std Err of Y Est	0.054133
R Squared	0.997094
No. of Observations	77
Degrees of Freedom	75

Terrestrial Intensity	
Minimum	1747
Maximum	1890
Mean	1839.259
Std.	37.66

Ko Coefficient(s)	0.298870
Std Err of Coef.	0.001862

Site 4, Date 910713, Time: (0928–1030)
Discharge 142 m^3/s
Location: 50 km

Regression Output:	
Constant	7.559331
Std Err of Y Est	0.087489
R Squared	0.990570
No. of Observations	64
Degrees of Freedom	62

Terrestrial Intensity	
Minimum	1566
Maximum	1715
Mean	1646.187
Std.	44.212

Ko Coefficient(s)	0.358679
Std Err of Coef.	0.004444

Site 5, Date 910524, Time: (1512–1535)
Discharge 425 m^3/s
Location: 77.61 km

Regression Output:	
Constant	6.360632
Std Err of Y Est	0.126415
R Squared	0.977043
No. of Observations	11
Degrees of Freedom	9

Terrestrial Intensity	
Minimum	403
Maximum	544
Mean	489.427
Std.	48.571

Ko Coefficient(s) 0.388773
Std Err of Coef. 0.019864

Site 5, Date 910713, Time: (1325–1413)
Discharge 142 m^3/s
Location: 77.61 km

Regression Output:	
Constant	7.719158
Std Err of Y Est	0.093288
R Squared	0.995136
No. of Observations	94
Degrees of Freedom	92

Terrestrial Intensity	
Minimum	1876
Maximum	1974
Mean	1928.2
Std.	27.403

Ko Coefficient(s) 0.343336
Std Err of Coef. 0.002502

Site 6, Date 910525, Time: (0932–1000)
Discharge 425 m^3/s
Location: 99.5 km

Regression Output:	
Constant	7.590677
Std Err of Y Est	0.064566
R Squared	0.991568
No. of Observations	53
Degrees of Freedom	51

Terrestrial Intensity	
Minimum	1604
Maximum	1732
Mean	1678.528
Std.	24.78

Ko Coefficient(s) 0.350981
Std Err of Coef. 0.004532

Site 6, Date 910714, Time: (0921–1005)
Discharge 142 m^3/s
Location: 99.5 km

Regression Output:	
Constant	7.538938
Std Err of Y Est	0.056397
R Squared	0.991742
No. of Observations	47
Degrees of Freedom	45

Terrestrial Intensity	
Minimum	1430
Maximum	1573
Mean	1498.5
Std.	42.601

Ko Coefficient(s) 0.347755
Std Err of Coef. 0.004730

Site 7, Date 910525, Time: (1311–1345)
Discharge 425 m^3/s
Location: 122.83 km

Regression Output:	
Constant	7.850438
Std Err of Y Est	0.094655
R Squared	0.991608
No. of Observations	66
Degrees of Freedom	64

Terrestrial Intensity	
Minimum	2052
Maximum	2198
Mean	2131.696
Std.	34.036

Ko Coefficient(s) 0.392197
Std Err of Coef. 0.004509

Site 7, Date 910714, Time: (1245–1321)
Discharge 142 m^3/s
Location: 122.83 km

Regression Output:	
Constant	7.701544
Std Err of Y Est	0.045699
R Squared	0.996210
No. of Observations	69
Degrees of Freedom	67

Terrestrial Intensity	
Minimum	2122
Maximum	2270
Mean	2199
Std.	42.712

Ko Coefficient(s) 0.280207
Std Err of Coef. 0.002111

Site 8, Date 910525, Time: (1423–1459)
Discharge 425 m^3/s
Location: 128.56 km

Regression Output:		Terrestrial Intensity	
Constant	7.821427	Minimum	1801
Std Err of Y Est	0.091055	Maximum	1939
R Squared	0.994377	Mean	1860.9
No. of Observations	30	Std.	40.088
Degrees of Freedom	28		
Ko Coefficient(s)	0.465453		
Std Err of Coef.	0.006614		

Site 8, Date 910715, Time: (1415–1533)
Discharge 142 m^3/s
Location: 128.56 km

Regression Output:		Terrestrial Intensity	
Constant	7.756251	Minimum	1745
Std Err of Y Est	0.038054	Maximum	1893
R Squared	0.998245	Mean	1828.1
No. of Observations	50	Std.	50.256
Degrees of Freedom	48		
Ko Coefficient(s)	0.348634		
Std Err of Coef.	0.002109		

Site 9, Date 910526, Time: (1032–1107)
Discharge 425 m^3/s
Location: 149.38 km

Regression Output:		Terrestrial Intensity	
Constant	7.833957	Minimum	1787
Std Err of Y Est	0.125566	Maximum	1920
R Squared	0.996179	Mean	1866.305
No. of Observations	72	Std.	37.475
Degrees of Freedom	70		
Ko Coefficient(s)	0.688990		
Std Err of Coef.	0.005100		

Site 9, Date 910715, Time: (1042–1137)
Discharge 142 m^3/s
Location: 149.38 km

Regression Output:		Terrestrial Intensity	
Constant	7.741661	Minimum	1751
Std Err of Y Est	0.100084	Maximum	1900
R Squared	0.996959	Mean	1816.7
No. of Observations	75	Std.	43.878
Degrees of Freedom	73		
Ko Coefficient(s)	0.351247		
Std Err of Coef.	0.002270		

Site 10, Date 910526, Time: (1511–1542)
Discharge 425 m^3/s
Location: 165.47 km

Regression Output:		Terrestrial Intensity	
Constant	7.714170	Minimum	1450
Std Err of Y Est	0.188447	Maximum	1600
R Squared	0.994086	Mean	1534.236
No. of Observations	72	Std.	47.828
Degrees of Freedom	70		
Ko Coefficient(s)	0.706328		
Std Err of Coef.	0.006511		

Site 10, Date 910629, Time: (1011–1050)
Discharge 142 m^3/s
Location: 165.47 km

Regression Output:		Terrestrial Intensity	
Constant	7.655929	Minimum	1758
Std Err of Y Est	0.075293	Maximum	1906
R Squared	0.997454	Mean	1808.1
No. of Observations	86	Std.	74.673
Degrees of Freedom	84		
Ko Coefficient(s)	0.458096		
Std Err of Coef.	0.002524		

Site 13, Date 910527, Time: (1116–1140)
Discharge 425 m^3/s
Location: 200.38 km

Regression Output:	
Constant	8.265475
Std Err of Y Est	0.359879
R Squared	0.981036
No. of Observations	51
Degrees of Freedom	49

Terrestrial Intensity	
Minimum	1952
Maximum	2019
Mean	1983
Std.	15.3797

Ko Coefficient(s) 1.07666
Std Err of Coef. 0.021384

Site 13, Date 910629, Time: (1525–1603)
Discharge 142 m^3/s
Location: 200.38 km

Regression Output:	
Constant	7.561004
Std Err of Y Est	0.133153
R Squared	0.994166
No. of Observations	69
Degrees of Freedom	67

Terrestrial Intensity	
Minimum	1519
Maximum	1667
Mean	1597.8
Std.	44.825

Ko Coefficient(s) 0.538365
Std Err of Coef. 0.005038

Site 14, Date 910527, Time: (1515–1549)
Discharge 425 m^3/s
Location: 224.03 km

Regression Output:	
Constant	7.739329
Std Err of Y Est	0.269485
R Squared	0.984589
No. of Observations	62
Degrees of Freedom	60

Terrestrial Intensity	
Minimum	1462
Maximum	1612
Mean	1531.854
Std.	53.107

Ko Coefficient(s) 0.893091
Std Err of Coef. 0.014424

Site 14, Date 910630, Time: (0856–0925)
Discharge 142 m^3/s
Location: 224.03 km

Regression Output:	
Constant	7.599766
Std Err of Y Est	0.082871
R Squared	0.996434
No. of Observations	57
Degrees of Freedom	55

Terrestrial Intensity	
Minimum	1331
Maximum	1481
Mean	1361.6
Std.	47.582

Ko Coefficient(s) 0.526510
Std Err of Coef. 0.004246

Site 16, Date 910528, Time: (1005–1040)
Discharge 425 m^3/s
Location: 249.94 km

Regression Output:	
Constant	7.947494
Std Err of Y Est	0.162688
R Squared	0.993380
No. of Observations	51
Degrees of Freedom	49

Terrestrial Intensity	
Minimum	1684
Maximum	1809
Mean	1742.607
Std.	37.741

Ko Coefficient(s) 1.085479
Std Err of Coef. 0.012658

Site 16, Date 910630, Time: (1206–1225)
Discharge 142 m^3/s
Location: 249.94 km

Regression Output:	
Constant	7.938944
Std Err of Y Est	0.083529
R Squared	0.994006
No. of Observations	51
Degrees of Freedom	49

Terrestrial Intensity	
Minimum	2026
Maximum	2050
Mean	2043.6
Std.	5.365

Ko Coefficient(s) 0.575515
Std Err of Coef. 0.006384

Site 18, Date 910528, Time: (1439–1456)
Discharge 425 m^3/s
Location: 276.33 km

Regression Output:	
Constant	7.936153
Std Err of Y Est	0.191473
R Squared	0.993558
No. of Observations	60
Degrees of Freedom	58

Terrestrial Intensity	
Minimum	1612
Maximum	1702
Mean	1657.55
Std.	28.353

Ko Coefficient(s)	1.092970
Std Err of Coef.	0.011555

Site 18, Date 910630, Time: (1447–1513)
Discharge 142 m^3/s
Location: 276.33 km

Regression Output:	
Constant	7.851642
Std Err of Y Est	0.062800
R Squared	0.998281
No. of Observations	64
Degrees of Freedom	62

Terrestrial Intensity	
Minimum	1672
Maximum	1808
Mean	1741.7
Std.	32.645

Ko Coefficient(s)	0.611572
Std Err of Coef.	0.003222

Site 20, Date 910529, Time: (1036–1056)
Discharge 425 m^3/s
Location: 291.61 km

Regression Output:	
Constant	7.908364
Std Err of Y Est	0.101961
R Squared	0.994603
No. of Observations	52
Degrees of Freedom	50

Terrestrial Intensity	
Minimum	1744
Maximum	1819
Mean	1782.096
Std.	23.4596

Ko Coefficient(s)	0.734972
Std Err of Coef.	0.007656

Site 20, Date 910701, Time: (0953–1023)
Discharge 142 m^3/s
Location: 291.61 km

Regression Output:	
Constant	7.753634
Std Err of Y Est	0.058755
R Squared	0.996861
No. of Observations	58
Degrees of Freedom	56

Terrestrial Intensity	
Minimum	1623
Maximum	1753
Mean	1686.5
Std.	41.418

Ko Coefficient(s)	0.492852
Std Err of Coef.	0.003695

Site 21, Date 910529, Time: (1503–1523)
Discharge 425 m^3/s
Location: 321.06 km

Regression Output:	
Constant	8.033757
Std Err of Y Est	0.363721
R Squared	0.988901
No. of Observations	52
Degrees of Freedom	50

Terrestrial Intensity	
Minimum	1448
Maximum	1591
Mean	1535.961
Std.	44.632

Ko Coefficient(s)	1.168774
Std Err of Coef.	0.017510

Site 21, Date 910701, Time: (1425–1506)
Discharge 142 m^3/s
Location: 321.06 km

Regression Output:	
Constant	7.886510
Std Err of Y Est	0.935055
R Squared	0.861380
No. of Observations	79
Degrees of Freedom	77

Terrestrial Intensity	
Minimum	1728
Maximum	1873
Mean	1801.1
Std.	43.137

Ko Coefficient(s)	0.644801
Std Err of Coef.	0.029477

ATTENUATION COEFFICIENT, K_o, SCALAR IRRADIANCE

Site 22, Date 910530, Time: (1012–1039)
Discharge 425 m^3/s
Location: 350.18 km

Regression Output:		Terrestrial Intensity	
Constant	7.843190	Minimum	1707
Std Err of Y Est	0.097131	Maximum	1816
R Squared	0.998185	Mean	1765.588
No. of Observations	68	Std.	31.795
Degrees of Freedom	66		

Ko Coefficient(s)	0.923394
Std Err of Coef.	0.004846

Site 22, Date 910702, Time: (0852–0934)
Discharge 142 m^3/s
Location: 350.18 km

Regression Output:		Terrestrial Intensity	
Constant	7.611927	Minimum	1333
Std Err of Y Est	0.086006	Maximum	1482
R Squared	0.998075	Mean	1407.4
No. of Observations	66	Std.	40.076
Degrees of Freedom	64		

Ko Coefficient(s)	0.568634
Std Err of Coef.	0.003121

Site 23, Date 910530, Time: (1411–1501)
Discharge 425 m^3/s
Location: 374.15 km

Regression Output:		Terrestrial Intensity	
Constant	7.910833	Minimum	1742
Std Err of Y Est	0.111755	Maximum	1899
R Squared	0.997171	Mean	1839.26
No. of Observations	46	Std.	34.621
Degrees of Freedom	44		

Ko Coefficient(s)	0.926508
Std Err of Coef.	0.007439

Site 23, Date 910702, Time: (1314–1348)
Discharge 142 m^3/s
Location: 374.15 km

Regression Output:		Terrestrial Intensity	
Constant	7.992922	Minimum	2003
Std Err of Y Est	0.085299	Maximum	2082
R Squared	0.996696	Mean	2030
No. of Observations	61	Std.	17.363
Degrees of Freedom	59		

Ko Coefficient(s)	0.66145
Std Err of Coef.	0.004957

Site 24, Date 910531, Time: (1000–1020)
Discharge 425 m^3/s
Location: 387.51 km

Regression Output:		Terrestrial Intensity	
Constant	5.893988	Minimum	223.2
Std Err of Y Est	0.198175	Maximum	361.7
R Squared	0.989643	Mean	230.7
No. of Observations	40	Std.	36.628
Degrees of Freedom	38		

Ko Coefficient(s)	1.033104
Std Err of Coef.	0.017144

Site 24, Date 910702, Time: (1513–1541)
Discharge 142 m^3/s
Location: 387.51 km

Regression Output:		Terrestrial Intensity	
Constant	7.812365	Minimum	1553
Std Err of Y Est	0.062675	Maximum	1703
R Squared	0.998102	Mean	1637.1
No. of Observations	59	Std.	48.546
Degrees of Freedom	57		

Ko Coefficient(s)	0.665269
Std Err of Coef.	0.003842

ATTENUATION COEFFICIENT, K_d, COSINE CORRECTED

Site 1, Date 910523, Time: (1129–1215)
Discharge 425 m^3/s
Location: 0.0 km

Regression Output:	
Constant	7.430618
Std Err of Y Est	0.151868
R Squared	0.963605
No. of Observations	76
Degrees of Freedom	74

Terrestrial Intensity	
Minimum	1964
Maximum	2068
Mean	2021.934
Std.	25.218

Kd Coefficient(s)	0.230401
Std Err of Coef.	0.005205

Site 1, Date 910628, Time: (1339–1458)
Discharge 142 m^3/s
Location: 0.0 km

Regression Output:	
Constant	7.333657
Std Err of Y Est	0.114991
R Squared	0.980678
No. of Observations	63
Degrees of Freedom	61

Terrestrial Intensity	
Minimum	1848
Maximum	1989
Mean	1918.158
Std.	43.959

Kd Coefficient(s)	0.227317
Std Err of Coef.	0.004085

Site 1, Date 911216, Time: (1239–1317)
Discharge 376–396 m^3/s
Location: 0.0 km

Regression Output:	
Constant	5.560097
Std Err of Y Est	0.149289
R Squared	0.965903
No. of Observations	330
Degrees of Freedom	328

Terrestrial Intensity	
Minimum	244
Maximum	386.6
Mean	289.6415
Std.	34.40311

Kd Coefficient(s)	0.33675
Std Err of Coef.	0.89334

Site 1, Date 910712, Time: (0925–1018)
Discharge 142 m^3/s
Location: 0.0 km

Regression Output:	
Constant	7.200940
Std Err of Y Est	0.102471
R Squared	0.992021
No. of Observations	56
Degrees of Freedom	54

Terrestrial Intensity	
Minimum	1505
Maximum	1651
Mean	1593.553
Std.	43.606

Kd Coefficient(s)	0.273746
Std Err of Coef.	0.003340

Site 2, Date 910523, Time: (1300–1337)
Discharge 425 m^3/s
Location: 23.8 km

Regression Output:	
Constant	7.400079
Std Err of Y Est	0.091952
R Squared	0.982008
No. of Observations	72
Degrees of Freedom	70

Terrestrial Intensity	
Minimum	1969
Maximum	2049
Mean	2017.375
Std.	16.68

Kd Coefficient(s)	0.246884
Std Err of Coef.	0.003994

Site 2, Date 910712, Time: (1127–1213)
Discharge 142 m^3/s
Location: 23.8 km

Regression Output:	
Constant	7.474100
Std Err of Y Est	0.043000
R Squared	0.996700
No. of Observations	82
Degrees of Freedom	80

Terrestrial Intensity	
Minimum	1931
Maximum	2032
Mean	1990.524
Std.	26.379

Kd Coefficient(s)	0.249889
Std Err of Coef.	0.001607

ATTENUATION COEFFICIENT, K_d, COSINE CORRECTED

Site 2, Date 910711, Time: (1334–1413)
Discharge 759–770 m^3/s
Location: 23.8 km

Regression Output:	
Constant	7.37234
Std Err of Y Est	0.22852
R Squared	0.874816
No. of Observations	41
Degrees of Freedom	39

Terrestrial Intensity	
Minimum	1906
Maximum	2006
Mean	1947.024
Std.	30.503

Kd Coefficient(s)	0.32034
Std Err of Coef.	0.019404

Site 3, Date 910523

NO DATA COLLECTED

Site 3, Date 910712, Time: (1433–1524)
Discharge 142 m^3/s
Location: 27.74 km

Regression Output:	
Constant	7.273514
Std Err of Y Est	0.122103
R Squared	0.969036
No. of Obs	57
Degrees of	55

Terrestrial Intensity	
Minimum	1624
Maximum	1773
Mean	1681.578
Std.	43.587

Kd Coefficient(s)	0.323267
Std Err of Coef.	0.007791

Site 4, Date 910524, Time: (1101–1131)
Discharge 425 m^3/s
Location: 50 km

Regression Output:	
Constant	7.463962
Std Err of Y Est	0.054627
R Squared	0.997157
No. of Observations	80
Degrees of Freedom	78

Terrestrial Intensity	
Minimum	1884
Maximum	1992
Mean	1960.462
Std.	19.007

Kd Coefficient(s)	0.314592
Std Err of Coef.	0.001901

Site 4, Date 910713, Time: (0928–1030)
Discharge 142 m^3/s
Location: 50 km

Regression Output:	
Constant	7.241084
Std Err of Y Est	0.101877
R Squared	0.989854
No. of Observations	55
Degrees of Freedom	53

Terrestrial Intensity	
Minimum	1505
Maximum	1654
Mean	1579.963
Std.	47.65

Kd Coefficient(s)	0.380370
Std Err of Coef.	0.005289

ATTENUATION COEFFICIENT, K_d, COSINE CORRECTED

Site 5, Date 910524, Time: (1417–1503)
Discharge 425 m^3/s
Location: 77.61 km

Regression Output:	
Constant	7.464023
Std Err of Y Est	0.053442
R Squared	0.995439
No. of Observations	14
Degrees of Freedom	12
Kd Coefficient(s)	0.398451
Std Err of Coef.	0.007785

Terrestrial Intensity	
Minimum	1900
Maximum	2047
Mean	1944.071
Std.	45.071

Site 5, Date 910713, Time: (1325–1413)
Discharge 142 m^3/s
Location: 77.61 km

Regression Output:	
Constant	7.405623
Std Err of Y Est	0.101746
R Squared	0.995202
No. of Observations	98
Degrees of Freedom	96
Kd Coefficient(s)	0.367692
Std Err of Coef.	0.002605

Terrestrial Intensity	
Minimum	1876
Maximum	1974
Mean	1928.357
Std.	27.757

Site 6, Date 910525, Time: (1009–1035)
Discharge 425 m^3/s
Location: 99.5 km

Regression Output:	
Constant	7.411833
Std Err of Y Est	0.054608
R Squared	0.995141
No. of Observations	33
Degrees of Freedom	31
Kd Coefficient(s)	0.368111
Std Err of Coef.	0.004619

Terrestrial Intensity	
Minimum	1756
Maximum	1895
Mean	1832.696
Std.	41.647

Site 6, Date 910714, Time: (0921–1005)
Discharge 142 m^3/s
Location: 99.5 km

Regression Output:	
Constant	7.237072
Std Err of Y Est	0.079750
R Squared	0.988721
No. of Observations	51
Degrees of Freedom	49
Kd Coefficient(s)	0.399570
Std Err of Coef.	0.006096

Terrestrial Intensity	
Minimum	1430
Maximum	1573
Mean	1497.784
Std.	42.878

Site 7, Date 910525

NO DATA COLLECTED

Site 7, Date 910714, Time: (1245–1321)
Discharge 142 m^3/s
Location: 122.83 km

Regression Output:	
Constant	7.565349
Std Err of Y Est	0.062718
R Squared	0.995109
No. of Observations	71
Degrees of Freedom	69
Kd Coefficient(s)	0.317502
Std Err of Coef.	0.002679

Terrestrial Intensity	
Minimum	2141
Maximum	2285
Mean	2207.873
Std.	40.206

ATTENUATION COEFFICIENT, K_d, COSINE CORRECTED

Site 8, Date 910525, Time: (1510–1540)
Discharge 425 m^3/s
Location: 128.56 km

Regression Output:	
Constant	7.322197
Std Err of Y Est	0.119274
R Squared	0.991418
No. of Observations	44
Degrees of Freedom	42
Kd Coefficient(s)	0.506195
Std Err of Coef.	0.007266

Terrestrial Intensity	
Minimum	1543
Maximum	1682
Mean	1605.045
Std.	38.373

Site 8, Date 910714, Time: (1415–1533)
Discharge 142 m^3/s
Location: 128.56 km

Regression Output:	
Constant	7.466106
Std Err of Y Est	0.045507
R Squared	0.997992
No. of Observations	51
Degrees of Freedom	49
Kd Coefficient(s)	0.378790
Std Err of Coef.	0.002427

Terrestrial Intensity	
Minimum	1745
Maximum	1893
Mean	1827.843
Std.	49.812

Site 9, Date 910526, Time: (1115–1143)
Discharge 425 m^3/s
Location: 149.38 km

Regression Output:	
Constant	7.561991
Std Err of Y Est	0.281489
R Squared	0.987490
No. of Observations	88
Degrees of Freedom	86
Kd Coefficient(s)	0.769448
Std Err of Coef.	0.009338

Terrestrial Intensity	
Minimum	1900
Maximum	2005
Mean	1962.204
Std.	23.694

Site 9, Date 910715, Time: (1024–1137)
Discharge 142 m^3/s
Location: 149.38 km

Regression Output:	
Constant	7.321053
Std Err of Y Est	0.155348
R Squared	0.992167
No. of Observations	75
Degrees of Freedom	73
Kd Coefficient(s)	0.338860
Std Err of Coef.	0.003523

Terrestrial Intensity	
Minimum	1751
Maximum	1900
Mean	1816.786
Std.	43.878

Site 10, Date 910526, Time: (1558–1606)
Discharge 425 m^3/s
Location: 165.47 km

Regression Output:	
Constant	7.215061
Std Err of Y Est	0.126055
R Squared	0.998067
No. of Observations	26
Degrees of Freedom	24
Kd Coefficient(s)	0.742538
Std Err of Coef.	0.006669

Terrestrial Intensity	
Minimum	1298
Maximum	1383
Mean	1366.076
Std.	17.018

Site 10, 910629, Time: (1011–1050)
Discharge 142 m^3/s
Location: 165.47 km

Regression Output:	
Constant	7.288689
Std Err of Y Est	0.133975
R Squared	0.993367
No. of Observations	74
Degrees of Freedom	72
Kd Coefficient(s)	0.467770
Std Err of Coef.	0.004504

Terrestrial Intensity	
Minimum	1728
Maximum	1877
Mean	1802.378
Std.	39.256

ATTENUATION COEFFICIENT, K_d, COSINE CORRECTED

Site 13, Date 910527, Time: (1149–1209)
Discharge 425 m^3/s
Location: 200.38 km

Regression Output:	
Constant	7.815037
Std Err of Y Est	0.270699
R Squared	0.988256
No. of Observations	61
Degrees of Freedom	59
Kd Coefficient(s)	1.073789
Std Err of Coef.	0.015238

Terrestrial Intensity	
Minimum	2003
Maximum	2032
Mean	2015.606
Std.	9.094

Site 13, Date 910629, Time: (1525–1603)
Discharge 142 m^3/s
Location: 200.38 km

Regression Output:	
Constant	7.189594
Std Err of Y Est	0.176751
R Squared	0.991040
No. of Observations	65
Degrees of Freedom	63
Kd Coefficient(s)	0.553968
Std Err of Coef.	0.006636

Terrestrial Intensity	
Minimum	1550
Maximum	1698
Mean	1618.523
Std.	40.919

Site 14, Date 910527, Time: (1557–1618)
Discharge 425 m^3/s
Location: 224.03 km

Regression Output:	
Constant	7.072127
Std Err of Y Est	0.204789
R Squared	0.994225
No. of Observations	46
Degrees of Freedom	44
Kd Coefficient(s)	1.049515
Std Err of Coef.	0.012058

Terrestrial Intensity	
Minimum	1254
Maximum	1404
Mean	1334.565
Std.	42.997

Site 14, Date 910630, Time: (0856–0925)
Discharge 142 m^3/s
Location: 224.03 km

Regression Output:	
Constant	7.100522
Std Err of Y Est	0.084724
R Squared	0.997251
No. of Observations	62
Degrees of Freedom	60
Kd Coefficient(s)	0.542361
Std Err of Coef.	0.003675

Terrestrial Intensity	
Minimum	1293
Maximum	1441
Mean	1373.79
Std.	49.689

Site 16, Date 910528, Time: (1047–1114)
Discharge 425 m^3/s
Location: 249.94 km

Regression Output:	
Constant	7.502784
Std Err of Y Est	0.335454
R Squared	0.973593
No. of Observations	55
Degrees of Freedom	53
Kd Coefficient(s)	1.001784
Std Err of Coef.	0.022662

Terrestrial intensity	
Minimum	1819
Maximum	1898
Mean	1862.036
Std.	24.318

Site 16, Date 910630, Time: (1206–1225)
Discharge 142 m^3/s
Location: 249.94 km

Regression Output:	
Constant	7.692370
Std Err of Y Est	0.155124
R Squared	0.985056
No. of Observations	55
Degrees of Freedom	53
Kd Coefficient(s)	0.643672
Std Err of Coef.	0.010889

Terrestrial Intensity	
Minimum	2026
Maximum	2052
Mean	2043.69
Std.	5.605

Site 18, Date 910528, Time: (1502–1518)
Discharge 425 m^3/s
Location: 276.33 km

Regression Output:	
Constant	7.306053
Std Err of Y Est	0.250936
R Squared	0.990056
No. of Observations	58
Degrees of Freedom	56
Kd Coefficient(s)	1.128186
Std Err of Coef.	0.015108

Terrestrial Intensity	
Minimum	1499
Maximum	1578
Mean	1540.379
Std.	25.079

Site 18, Date 910630, Time: (1447–1513)
Discharge 142 m^3/s
Location: 276.33 km

Regression Output:	
Constant	7.337508
Std Err of Y Est	0.105094
R Squared	0.995562
No. of Observations	68
Degrees of Freedom	66
Kd Coefficient(s)	0.613211
Std Err of Coef.	0.005039

Terrestrial Intensity	
Minimum	1672
Maximum	1808
Mean	1741.661
Std.	32.811

Site 20, Date 910529, Time: (1104–1122)
Discharge 425 m^3/s
Location: 291.61 km

Regression Output:	
Constant	7.588494
Std Err of Y Est	0.073488
R Squared	0.997353
No. of Observations	52
Degrees of Freedom	50
Kd Coefficient(s)	0.752832
Std Err of Coef.	0.005484

Terrestrial Intensity	
Minimum	1837
Maximum	1892
Mean	1864.134
Std.	16.085

Site 20, Date 910701, Time: (0953–1023)
Discharge 142 m^3/s
Location: 291.61 km

Regression Output:	
Constant	7.393184
Std Err of Y Est	0.060133
R Squared	0.997395
No. of Observations	62
Degrees of Freedom	60
Kd Coefficient(s)	0.530677
Std Err of Coef.	0.003500

Terrestrial Intensity	
Minimum	1623
Maximum	1753
Mean	1686.274
Std.	40.877

Site 21, Date 910529, Time: (1529–1552)
Discharge 425 m^3/s
Location: 321.06 km

Regression Output:	
Constant	7.319699
Std Err of Y Est	0.331507
R Squared	0.990139
No. of Observations	76
Degrees of Freedom	74
Kd Coefficient(s)	1.130883
Std Err of Coef.	0.013118

Terrestrial Intensity	
Minimum	1322
Maximum	1472
Mean	1412.657
Std.	46.516

Site 21, Date 910701, Time: (1425–1506)
Discharge 142 m^3/s
Location: 321.06 km

Regression Output:	
Constant	7.346620
Std Err of Y Est	0.114777
R Squared	0.997175
No. of Observations	78
Degrees of Freedom	76
Kd Coefficient(s)	0.599647
Std Err of Coef.	0.003661

Terrestrial Intensity	
Minimum	1728
Maximum	1873
Mean	1800.717
Std.	43.18

ATTENUATION COEFFICIENT, K_d, COSINE CORRECTED

Site 22, Date 910530, Time: (1047–1116)
Discharge 425 m^3/s
Location: 350.18 km

Regression Output:	
Constant	7.450815
Std Err of Y Est	0.103711
R Squared	0.997989
No. of Observations	68
Degrees of Freedom	66
Kd Coefficient(s)	0.933231
Std Err of Coef.	0.005155

Terrestrial Intensity	
Minimum	1809
Maximum	1917
Mean	1873
Std.	30.794

Site 22, Date 910702, Time: (0852–0934)
Discharge 142 m^3/s
Location: 350.18 km

Regression Output:	
Constant	7.058595
Std Err of Y Est	0.123258
R Squared	0.996151
No. of Observations	67
Degrees of Freedom	65
Kd Coefficient(s)	0.560595
Std Err of Coef.	0.004321

Terrestrial Intensity	
Minimum	1333
Maximum	1480
Mean	1406.059
Std.	38.73

Site 23, Date 910530, Time: (1510–1536)
Discharge 425 m^3/s
Location: 374.15 km

Regression Output:	
Constant	7.219155
Std Err of Y Est	0.150779
R Squared	0.995973
No. of Observations	62
Degrees of Freedom	60
Kd Coefficient(s)	1.046712
Std Err of Coef.	0.008591

Terrestrial Intensity	
Minimum	1487
Maximum	1665
Mean	1551.935
Std.	37.102

Site 23, Date 910702, Time: (1314–1348)
Discharge 142 m^3/s
Location: 374.15 km

Regression Output:	
Constant	7.584349
Std Err of Y Est	0.093657
R Squared	0.996600
No. of Observations	66
Degrees of Freedom	64
Kd Coefficient(s)	0.678084
Std Err of Coef.	0.004950

Terrestrial intensity	
Minimum	1992
Maximum	2082
Mean	2029.772
Std.	17.656

Site 24, Date 910531, Time: (1028–1049)
Discharge 425 m^3/s
Location: 387.51 km

Regression Output:	
Constant	5.914626
Std Err of Y Est	0.160836
R Squared	0.994018
No. of Observations	42
Degrees of Freedom	40
Kd Coefficient(s)	1.079363
Std Err of Coef.	0.013238

Terrestrial Intensity	
Minimum	283.8
Maximum	430.4
Mean	351.807
Std.	42.822

Site 24, Date 910702, Time: (1513–1541)
Discharge 142 m^3/s
Location: 387.51 km

Regression Output:	
Constant	7.378757
Std Err of Y Est	0.074423
R Squared	0.997813
No. of Observations	62
Degrees of Freedom	60
Kd Coefficient(s)	0.690052
Std Err of Coef.	0.004170

Terrestrial Intensity	
Minimum	1550
Maximum	1699
Mean	1632.709
Std.	48.681

ATTENUATION COEFFICIENT, K_d, COSINE CORRECTED

Paria Tributary, Date 911106, Time: (1119–1355)
Discharge .34–.33 m^3/s

Regression Output:		Terrestrial Intensity	
Constant	7.432745	Minimum	1143
Std Err of Y Est	1.333641	Maximum	1337
R Squared	0.824102	Mean	1258.406
No. of Observations	229	Std.	60.11144
Degrees of Freedom	227		

Kd Coefficient(s)	29.1333
Std Err of Coef.	0.89334